An augmented velocity–vorticity–pressure formulation for the Brinkman equations

Verónica Anaya[1], Gabriel N. Gatica[2,3,*,†], David Mora[1,2] and Ricardo Ruiz-Baier[4]

[1]*Departamento de Matemática, Facultad de Ciencias, Universidad del Bío-Bío, Casilla 5-C, Concepción, Chile*
[2]*Centro de Investigación en Ingeniería Matemática (CI²MA), Universidad de Concepción, Concepción, Chile*
[3]*Departamento de Ingeniería Matemática, Universidad de Concepción, Casilla 160-C, Concepción, Chile*
[4]*Institute of Earth Sciences, Géopolis UNIL-Mouline, University of Lausanne, Lausanne CH-1015, Switzerland*

SUMMARY

This paper deals with the analysis of a new augmented mixed finite element method in terms of vorticity, velocity, and pressure, for the Brinkman problem with nonstandard boundary conditions. The approach is based on the introduction of Galerkin least-squares terms arising from the constitutive equation relating the aforementioned unknowns and from the incompressibility condition. We show that the resulting augmented bilinear form is continuous and elliptic, which, thanks to the Lax–Milgram theorem, and besides proving the well-posedness of the continuous formulation, ensures the solvability and stability of the Galerkin scheme with any finite element subspace of the continuous space. In particular, Raviart–Thomas elements of any order $k \geqslant 0$ for the velocity field, and piecewise continuous polynomials of degree $k+1$ for both the vorticity and the pressure, can be utilized. A priori error estimates and the corresponding rates of convergence are also given here. Next, we derive two reliable and efficient residual-based a posteriori error estimators for this problem. The ellipticity of the bilinear form together with the local approximation properties of the Clément interpolation operator are the main tools for showing the reliability. In turn, inverse inequalities and the localization technique based on triangle-bubble and edge-bubble functions are utilized to show the efficiency. Finally, several numerical results illustrating the good performance of the method, confirming the properties of the estimators and showing the behavior of the associated adaptive algorithms, are reported. Copyright © 2015 John Wiley & Sons, Ltd.

1. INTRODUCTION

We are interested in the numerical approximation of the velocity–vorticity–pressure formulation of the linear Brinkman (or generalized Stokes) problem. These equations can be considered as an extension of Darcy's law to describe the laminar flow behavior of a viscous fluid within a porous material with possibly heterogeneous permeability, so that the flow is dominated by Darcy regime in some regions and by Stokes elsewhere. Another instance where the Brinkman problem is encountered is after time discretizations of transient Stokes equations modelling the motion of an incompressible free fluid. In any case, the accurate and efficient approximation of viscous flow governed by Brinkman equations is of high practical importance and has been a main focus of research in several industrial and environmental applications, including the study of foams, filtering porous

---

*Correspondence to: Gabriel N. Gatica, CI²MA and Departamento de Ingeniería Matemática, Universidad de Concepción, Casilla 160-C, Concepción, Chile.
†E-mail: ggatica@ci2ma.udec.cl

layers, oil reservoirs, or heat pipes. Moreover, in addition to velocity and pressure, other intrinsic fields are typically required to examine flow patterns, such as vorticity or shear stresses.

The mathematical analysis and the numerical discretization of the Brinkman problem inherit all the well-known difficulties associated with both Darcy and Stokes equations. A number of robust solvers for general saddle-point problems and numerical methods have been introduced for the Brinkman system in the last few years, and most of them are based on mixed finite element formulations deriving from Stokes-based methods and making extensive use of diverse stabilization techniques introduced either to comply with or to circumvent the discrete inf-sup condition. In particular, a continuous penalty method has been proposed and analyzed in [1]. Also, a pressure gradient stabilization method for the generalized Stokes problem has been introduced in [2]. In the context of mixed finite elements, we cite [3], where a variational formulation that can be recast as a twofold saddle-point problem is constructed and analyzed. The approach in [3] is based on the introduction of the flux and the tensor gradient of the velocity as further unknowns, whereas the discrete method uses Raviart–Thomas spaces of order zero to approximate the flux and piecewise constant functions to approximate the velocity and the pressure. In that contribution, the authors prove that the continuous and discrete formulations are well posed and derive the associated a priori error analysis and a posteriori error estimates based on local problems. In [4], the pseudostress and the trace-free velocity gradient are introduced as auxiliary unknowns, and a pseudostress–velocity formulation is considered, for which existence, uniqueness, and error estimates are derived. More recently, dual-mixed methods based on the velocity–pseudostress and pseudostress have been introduced in [5] and [6], respectively, for the generalized Stokes problem. In the former, the approach from [7] (see also [8]) is adapted to propose an augmented mixed method in terms of velocity and pseudostress, for which optimal error estimates are proved. On the other hand, in [6], a formulation based only on the pseudostress is proposed for the Brinkman problem, thus simplifying and improving the analysis from [5]. The results in [6] include a priori and a posteriori error analyses of the resulting Galerkin scheme. With respect to the numerical study of Stokes and Navier–Stokes equations formulated in terms of vorticity–velocity–pressure fields, we mention the formulations based on least squares, stabilization techniques, mixed methods, spectral discretizations, and hybridizable discontinuous Galerkin, which can be found in [9–18] and the references in these papers. However, up to our knowledge, the Brinkman problem has been considered using mixed vorticity–velocity–pressure formulations only very recently [19], in where a dual-mixed formulation has been analyzed at the continuous and discrete levels using the Babuška–Brezzi theory and optimal error estimates are provided.

The so-called augmented mixed finite elements (also known as Galerkin least-squares methods [12, 20, 21]) can be regarded as a stabilization technique where some terms are added to the variational formulation so that, either the resulting augmented variational formulations are defined by strongly coercive bilinear forms (see, e.g., [22]), or they enable to bypass the kernel property, which is very difficult to obtain in practice, or they allow the fulfillment of the inf-sup condition at the continuous and discrete levels in mixed formulations ([23]). This approach has been considered in, for example, [5, 24–29] for Stokes, generalized Stokes (in velocity–pseudostress formulation), coupling of quasi-Newtonian fluids and porous media, and Navier–Stokes equations, and in [30] for an augmented mixed formulation applied to elliptic problems with mixed boundary conditions.

Here, we propose a new class of stabilized finite element approximations of the Brinkman equations, written in terms of the velocity, vorticity, and pressure fields. One of the main goals of the present approach is to build different families of finite elements to approximate the model problem with the liberty of choosing any combination of the finite element subspaces of the continuous spaces and extend recent results given in [24], where a new stabilized finite element approximation for the Stokes equations was analyzed using an extension of the Babuška–Brezzi theory (cf. [31, 32]). As compared with other approaches, in particular with the one from [6] that has been described previously, the proposed method also exhibits the advantage that the vorticity unknown (which is a sought quantity of practical interest) can be accessed directly, with the desired accuracy and without postprocessing. This property is difficult to obtain in methods written only in terms of vector potential and vorticity [15]. In addition, the approach of the present paper considers nonstandard boundary conditions, whereas the model in [6] is restricted to classical mixed boundary conditions.

On the other hand, differently from [6], where the resulting continuous formulation, being of saddle-point structure, falls into the framework of the Babuška–Brezzi theory, the present variational formulation is based on the introduction of suitable Galerkin least-squares terms, which let us analyze the problem by the classical Lax–Milgram theorem. Indeed, to ensure the existence and uniqueness of solution, at continuous and discrete levels, we prove that the corresponding resulting augmented bilinear form is continuous and elliptic. For the numerical approximation, we consider in particular the family of finite elements $\mathbf{RT}_k - P_{k+1} - P_{k+1}$, $k \geq 0$, that is, Raviart–Thomas elements of order k for the velocity field and piecewise continuous polynomials of degree $k + 1$ for the (scalar) vorticity and the pressure. We emphasize that the present approach extends for approximations of the pressure lying in any subspace of $\mathrm{H}^1(\Omega)$, which differs from the mixed method in [19] where the inf-sup condition needed for the stability of the corresponding Galerkin scheme only holds for certain subspaces of $\mathrm{L}^2(\Omega)$. Numerical experiments with the family of finite elements considered in this paper perform satisfactorily for a variety of boundary conditions. We also test the applicability of the present framework using the family of finite elements: $\mathbf{BDM}_{k+1} - P_{k+1} - P_{k+1}$, $k \geq 0$ that is, classical Brezzi–Douglas–Marini finite elements for the velocity field and piecewise continuous polynomials of degree $k + 1$ for the vorticity and the pressure. Certainly, as supported by the theory, one could employ any triple of finite element subspaces of the corresponding continuous spaces.

Outline. We have organized the contents of this paper as follows. In the remainder of this section, we introduce some standard notation and needed functional spaces, describe the boundary value problem of interest, and present the associate dual-mixed variational formulation, which will be modified to write our method. In Section 2, we set the stabilized variational formulation and then show that it is well posed using the classical Lax–Milgram theorem. In Section 3, we present the discrete method, provide particular families of stable finite elements, and obtain error estimates for the proposed methods. Section 4 is devoted to the reliability and efficiency analysis of two a posteriori error estimators. Finally, several numerical results assessing the performance of the methods, illustrating the convergence rates predicted by the theory, confirming the properties of the a posteriori error estimators, and showing the behavior of the associated adaptive algorithms, are collected in Section 5.

Preliminaries. Let us assume that $\Omega \subset \mathbb{R}^2$ is a bounded and simply connected Lipschitz domain. We denote by $\boldsymbol{n} = (n_i)_{1 \leq i \leq 2}$ the outward unit normal vector to the boundary $\Gamma := \partial\Omega$ and by $\boldsymbol{t} = (t_i)_{1 \leq i \leq 2}$ the unit tangent vector to $\partial\Omega$ oriented such that $t_1 = -n_2, t_2 = n_1$. Moreover, we assume that $\partial\Omega$ is polygonal and admits a disjoint partition $\partial\Omega = \Gamma \cup \Sigma$. For the sake of simplicity, we also assume that both Γ and Σ have positive measure.

For $s \geq 0$, the symbol $\|\cdot\|_{s,\Omega}$ stands for the norm of the Hilbertian Sobolev spaces $\mathrm{H}^s(\Omega)$ or $\mathbf{H}^s(\Omega) = [\mathrm{H}^s(\Omega)]^2$, with the convention $\mathrm{H}^0(\Omega) := \mathrm{L}^2(\Omega)$ and $\mathbf{H}^0(\Omega) = \mathbf{L}^2(\Omega)$. We also define the Hilbert space

$$\mathbf{H}(\mathrm{div}; \Omega) := \left\{ \boldsymbol{v} \in \mathbf{L}^2(\Omega) : \quad \mathrm{div}\, \boldsymbol{v} \in \mathrm{L}^2(\Omega) \right\},$$

whose norm is given by $\|\boldsymbol{v}\|_{\mathrm{div},\Omega}^2 := \|\boldsymbol{v}\|_{0,\Omega}^2 + \|\mathrm{div}\, \boldsymbol{v}\|_{0,\Omega}^2$. Hereafter, we use the following notation for any vector field $\boldsymbol{v} = (v_i)_{i=1,2}$ and any scalar field η:

$$\mathrm{div}\, \boldsymbol{v} := \partial_1 v_1 + \partial_2 v_2, \qquad \mathrm{rot}\, \boldsymbol{v} := \partial_1 v_2 - \partial_2 v_1, \qquad \nabla\eta := \begin{pmatrix} \partial_1 \eta \\ \partial_2 \eta \end{pmatrix}, \qquad \mathrm{curl}\, \eta := \begin{pmatrix} \partial_2 \eta \\ -\partial_1 \eta \end{pmatrix}.$$

In addition, we will denote with c and C, with or without subscripts, tildes, or hats, a generic constant independent of the mesh parameter h, which may take different values in different occurrences.

The model problem. The Brinkman (or generalized Stokes) problem [1, 5, 6], formulated in terms of the velocity $\boldsymbol{u}$, vorticity ω, and pressure p of an incompressible viscous fluid (see also [19]), reads as follows: given a force density $\boldsymbol{f}$ and a vector field $\boldsymbol{a}$, we seek a vector field $\boldsymbol{u}$, a scalar field ω, and a scalar field p such that

$$
\begin{cases}
\sigma \boldsymbol{u} + \nu \operatorname{curl} \omega + \nabla p = \boldsymbol{f} & \text{in } \Omega, \\
\omega - \operatorname{rot} \boldsymbol{u} = 0 & \text{in } \Omega, \\
\operatorname{div} \boldsymbol{u} = 0 & \text{in } \Omega, \\
\boldsymbol{u} \cdot \boldsymbol{t} = \boldsymbol{a} \cdot \boldsymbol{t} & \text{on } \Sigma, \\
p = 0 & \text{on } \Sigma, \\
\boldsymbol{u} \cdot \boldsymbol{n} = 0 & \text{on } \Gamma, \\
\omega = 0 & \text{on } \Gamma,
\end{cases}
\tag{1.1}
$$

where $\boldsymbol{u} \cdot \boldsymbol{t}$ and $\boldsymbol{u} \cdot \boldsymbol{n}$ stand for the normal and tangential components of the velocity, respectively. In the model, $\nu > 0$ is the kinematic viscosity of the fluid, and $\sigma > 0$ is a parameter representing the ratio between the fluid density and the permeability of the porous medium. In addition, we assume that a boundary compatibility condition holds, that is, there exists a velocity field $\boldsymbol{w} \in \mathrm{L}^2(\Omega)^2$ satisfying $\operatorname{div} \boldsymbol{w} = 0$ a.e. in Ω, $\boldsymbol{w} \cdot \boldsymbol{t} = \boldsymbol{a} \cdot \boldsymbol{t}$ on Σ and $\boldsymbol{w} \cdot \boldsymbol{n} = 0$ on Γ. For a detailed study on different types of standard and nonstandard boundary conditions for incompressible flows, we refer to [33, 34].

We remark that the following analysis to be developed can be easily extended to the case of nonhomogeneous boundary conditions for the pressure, normal velocity, and vorticity.

2. THE AUGMENTED VORTICITY–VELOCITY–PRESSURE FORMULATION

2.1. Variational formulations and preliminary results

In this section, we set the dual-mixed variational formulation of problem (1.1) and then propose a corresponding augmented approach. To this end, we first introduce the spaces

$$
\mathbf{H}_\Gamma(\operatorname{div}; \Omega) := \{ \boldsymbol{v} \in \mathbf{H}(\operatorname{div}; \Omega) : \boldsymbol{v} \cdot \boldsymbol{n} = 0 \text{ on } \Gamma \} \quad \text{and} \quad \mathrm{H}_\Gamma^1(\Omega) := \{ \eta \in \mathrm{H}^1(\Omega) : \eta = 0 \text{ on } \Gamma \},
$$

which are endowed with the natural norms, and denote by $\langle \cdot, \cdot \rangle_\Sigma$ the duality pairing between $\mathrm{H}^{-1/2}(\Sigma)$ and $\mathrm{H}^{1/2}(\Sigma)$ with respect to the $\mathrm{L}^2(\Sigma)$-inner product. Then, by testing system (1.1) with adequate functions and imposing the boundary conditions, we find that the dual-mixed variational formulation of (1.1) can be written as the twofold saddle-point problem (cf. [31, 32]): find $(\boldsymbol{u}, \omega, p) \in \mathbf{H}_\Gamma(\operatorname{div}; \Omega) \times \mathrm{H}_\Gamma^1(\Omega) \times \mathrm{L}^2(\Omega)$ such that

$$
\begin{aligned}
a(\boldsymbol{u}, \boldsymbol{v}) + b_1(\boldsymbol{v}, \omega) + b_2(p, \boldsymbol{v}) &= G(\boldsymbol{v}) && \forall \boldsymbol{v} \in \mathbf{H}_\Gamma(\operatorname{div}; \Omega), \\
b_1(\boldsymbol{u}, \eta) - d(\omega, \eta) &= F(\eta) && \forall \eta \in \mathrm{H}_\Gamma^1(\Omega), \\
b_2(q, \boldsymbol{u}) &= 0 && \forall q \in \mathrm{L}^2(\Omega),
\end{aligned}
\tag{2.1}
$$

where the bilinear forms $a : \mathbf{H}_\Gamma(\operatorname{div}; \Omega) \times \mathbf{H}_\Gamma(\operatorname{div}; \Omega) \to \mathbb{R}$, $b_1 : \mathbf{H}_\Gamma(\operatorname{div}; \Omega) \times \mathrm{H}_\Gamma^1(\Omega) \to \mathbb{R}$, $b_2 : \mathrm{L}^2(\Omega) \times \mathbf{H}_\Gamma(\operatorname{div}; \Omega) \to \mathbb{R}$, $d : \mathrm{H}_\Gamma^1(\Omega) \times \mathrm{H}_\Gamma^1(\Omega) \to \mathbb{R}$, and the linear functionals $G : \mathbf{H}_\Gamma(\operatorname{div}; \Omega) \to \mathbb{R}$, and $F : \mathrm{H}_\Gamma^1(\Omega) \to \mathbb{R}$ are defined by

$$
a(\boldsymbol{u}, \boldsymbol{v}) := \sigma \int_\Omega \boldsymbol{u} \cdot \boldsymbol{v}, \ b_1(\boldsymbol{v}, \eta) := \nu \int_\Omega \operatorname{curl} \eta \cdot \boldsymbol{v}, \ d(\omega, \eta) := \nu \int_\Omega \omega \eta, \ b_2(q, \boldsymbol{v}) := -\int_\Omega q \operatorname{div} \boldsymbol{v},
$$

and

$$
G(\boldsymbol{v}) := \int_\Omega \boldsymbol{f} \cdot \boldsymbol{v}, \qquad F(\eta) := -\nu \langle \boldsymbol{a} \cdot \boldsymbol{t}, \eta \rangle_\Sigma,
$$

for all $\boldsymbol{u}, \boldsymbol{v} \in \mathbf{H}_\Gamma(\operatorname{div}; \Omega)$, $\omega, \eta \in \mathrm{H}_\Gamma^1(\Omega)$, and $q \in \mathrm{L}^2(\Omega)$.

The well-posedness of (2.1) has been recently proved in [19]. In turn, the converse of the derivation of (2.1) is provided next. More precisely, the following theorem establishes that the unique solution of (2.1) solves the original boundary value problem (1.1).

Theorem 2.1
Let $(\boldsymbol{u}, \omega, p) \in \mathbf{H}_\Gamma(\mathrm{div}; \Omega) \times \mathrm{H}^1_\Gamma(\Omega) \times \mathrm{L}^2(\Omega)$ be the unique solution of (2.1). Then $\mathrm{div}\,\boldsymbol{u} = 0$ in Ω, $\omega = \mathrm{rot}\,\boldsymbol{u}$ in Ω, $\boldsymbol{u} \cdot \boldsymbol{t} = \boldsymbol{a} \cdot \boldsymbol{t}$ on Σ, $\sigma\boldsymbol{u} + \nu\,\mathrm{curl}\,\omega + \nabla p = \boldsymbol{f}$ in Ω (which yields $p \in H^1(\Omega)$) and $p = 0$ on Σ.

Proof
It follows by integrating backwardly in (2.1) and employing suitable test functions. Further details are omitted. □

Now, because p actually lives in the space $\mathrm{H}^1(\Omega)$, we suggest to enrich the aforementioned system (2.1) with residuals arising from the first and the third equations of system (1.1). This approach permits us to analyze the problem directly under the classical Lax–Milgram theorem. More precisely, we add to the system (2.1) the following Galerkin least-squares terms:

$$\kappa_1 \int_\Omega (\sigma\boldsymbol{u} + \nu\,\mathrm{curl}\,\omega + \nabla p - \boldsymbol{f}) \cdot \mathrm{curl}\,\eta = 0 \quad \forall \eta \in \mathrm{H}^1_\Gamma(\Omega),$$

$$\kappa_2 \int_\Omega (\sigma\boldsymbol{u} + \nu\,\mathrm{curl}\,\omega + \nabla p - \boldsymbol{f}) \cdot \nabla q = 0 \quad \forall q \in \mathrm{H}^1_\Sigma(\Omega), \qquad (2.2)$$

$$\kappa_3 \int_\Omega \mathrm{div}\,\boldsymbol{u}\,\mathrm{div}\,\boldsymbol{v} = 0 \quad \forall \boldsymbol{v} \in \mathbf{H}_\Gamma(\mathrm{div}; \Omega),$$

where κ_1, κ_2, and κ_3 are positive stabilization parameters to be specified later and

$$\mathrm{H}^1_\Sigma(\Omega) := \{q \in \mathrm{H}^1(\Omega): \quad q = 0 \text{ on } \Sigma\}.$$

Using an integration by parts, the fact that $\mathrm{div}\,\mathrm{curl}$ is the null operator, and the boundary conditions, we may rewrite the first two equations of (2.2) equivalently as follows:

$$\kappa_1\sigma \int_\Omega \boldsymbol{u} \cdot \mathrm{curl}\,\eta + \kappa_1\nu \int_\Omega \mathrm{curl}\,\omega \cdot \mathrm{curl}\,\eta = \kappa_1 \int_\Omega \boldsymbol{f} \cdot \mathrm{curl}\,\eta \quad \forall \eta \in \mathrm{H}^1_\Gamma(\Omega),$$

$$\kappa_2\sigma \int_\Omega \boldsymbol{u} \cdot \nabla q + \kappa_2 \int_\Omega \nabla p \cdot \nabla q = \kappa_2 \int_\Omega \boldsymbol{f} \cdot \nabla q \quad \forall q \in \mathrm{H}^1_\Sigma(\Omega).$$

In this way, we propose the following augmented variational formulation: find $\vec{\boldsymbol{u}} := (\boldsymbol{u}, \omega, p) \in \mathbb{H}$ such that

$$\mathcal{A}(\vec{\boldsymbol{u}}, \vec{\boldsymbol{v}}) = \mathcal{G}(\vec{\boldsymbol{v}}) \qquad \forall \vec{\boldsymbol{v}} := (\boldsymbol{v}, \eta, q) \in \mathbb{H}, \qquad (2.3)$$

where the space $\mathbb{H} := \mathbf{H}_\Gamma(\mathrm{div}; \Omega) \times \mathrm{H}^1_\Gamma(\Omega) \times \mathrm{H}^1_\Sigma(\Omega)$ is endowed with the corresponding product norm, and the bilinear form $\mathcal{A} : \mathbb{H} \times \mathbb{H} \to \mathbb{R}$ and the linear functional $\mathcal{G} : \mathbb{H} \to \mathbb{R}$ are defined by

$$\mathcal{A}(\vec{\boldsymbol{u}}, \vec{\boldsymbol{v}}) := \sigma \int_\Omega \boldsymbol{u} \cdot \boldsymbol{v} + \nu \int_\Omega \mathrm{curl}\,\omega \cdot \boldsymbol{v} - \int_\Omega p\,\mathrm{div}\,\boldsymbol{v} - \nu \int_\Omega \mathrm{curl}\,\eta \cdot \boldsymbol{u} + \nu \int_\Omega \omega\eta$$

$$+ \int_\Omega q\,\mathrm{div}\,\boldsymbol{u} + \kappa_1\sigma \int_\Omega \boldsymbol{u} \cdot \mathrm{curl}\,\eta + \kappa_1\nu \int_\Omega \mathrm{curl}\,\omega \cdot \mathrm{curl}\,\eta + \kappa_2\sigma \int_\Omega \boldsymbol{u} \cdot \nabla q \qquad (2.4)$$

$$+ \kappa_2 \int_\Omega \nabla p \cdot \nabla q + \kappa_3 \int_\Omega \mathrm{div}\,\boldsymbol{u}\,\mathrm{div}\,\boldsymbol{v},$$

and

$$\mathcal{G}(\vec{\boldsymbol{v}}) := \int_\Omega \boldsymbol{f} \cdot \boldsymbol{v} + \nu\langle\boldsymbol{a} \cdot \boldsymbol{t}, \eta\rangle_\Sigma + \kappa_1 \int_\Omega \boldsymbol{f} \cdot \mathrm{curl}\,\eta + \kappa_2 \int_\Omega \boldsymbol{f} \cdot \nabla q, \qquad (2.5)$$

for all $\vec{\boldsymbol{u}} := (\boldsymbol{u}, \omega, p)$, $\vec{\boldsymbol{v}} := (\boldsymbol{v}, \eta, q) \in \mathbb{H}$.

2.2. *Unique solvability of the augmented formulation*

Next, we will prove that our augmented variational formulation (2.3) satisfies the hypotheses of the Lax–Milgram theorem, that is, the idea is to choose κ_1, κ_2, and κ_3 so that the bilinear form $\mathcal{A}$ becomes strongly coercive on $\mathbb{H}$, which yields the unique solvability and continuous dependence on the data of this variational formulation. First, we observe that the bilinear form $\mathcal{A}$ and the linear functional $\mathcal{G}$ are bounded. More precisely, there exist C_1 and $C_2 > 0$ such that

$$
\begin{aligned}
|\mathcal{A}(\vec{w}, \vec{v})| &\leqslant C_1 \|\vec{w}\|_{\mathbb{H}} \|\vec{v}\|_{\mathbb{H}} && \forall\, \vec{w},\, \vec{v} \in \mathbb{H}\,, \\
|\mathcal{G}(\vec{v})| &\leqslant C_2 \left\{ \|\boldsymbol{a} \cdot \boldsymbol{t}\|_{-1/2,\Sigma} + \|\boldsymbol{f}\|_{0,\Omega} \right\} \|\vec{v}\|_{\mathbb{H}} && \forall\, \vec{v} \in \mathbb{H}\,.
\end{aligned}
\tag{2.6}
$$

The following lemma shows that the bilinear form $\mathcal{A}$ is $\mathbb{H}$-elliptic.

Lemma 2.2
Assume that $\kappa_1 \in (0, \frac{\nu}{\sigma})$, $\kappa_2 \in (0, \frac{1}{\sigma})$, and $\kappa_3 > 0$. Then, there exists $\alpha > 0$ such that

$$
\mathcal{A}(\vec{v}, \vec{v}) \geqslant \alpha \|\vec{v}\|_{\mathbb{H}}^2 \qquad \forall\, \vec{v} \in \mathbb{H}\,.
$$

Proof
According to the definition of $\mathcal{A}$ in (2.4) and applying the Cauchy–Schwarz inequality, we obtain

$$
\begin{aligned}
\mathcal{A}(\vec{v}, \vec{v}) &= \sigma\|\boldsymbol{v}\|_{0,\Omega}^2 + \nu\|\eta\|_{0,\Omega}^2 + \kappa_1\sigma\int_\Omega \operatorname{curl}\eta \cdot \boldsymbol{v} + \kappa_1\nu|\eta|_{1,\Omega}^2 + \kappa_2\sigma\int_\Omega \boldsymbol{v}\cdot\nabla q \\
&\quad + \kappa_2|q|_{1,\Omega}^2 + \kappa_3\|\operatorname{div}\boldsymbol{v}\|_{0,\Omega}^2 \\
&\geqslant \sigma\|\boldsymbol{v}\|_{0,\Omega}^2 + \nu\|\eta\|_{0,\Omega}^2 - \kappa_1\sigma|\eta|_{1,\Omega}\|\boldsymbol{v}\|_{0,\Omega} + \kappa_1\nu|\eta|_{1,\Omega}^2 - \kappa_2\sigma\|\boldsymbol{v}\|_{0,\Omega}|q|_{1,\Omega} \\
&\quad + \kappa_2|q|_{1,\Omega}^2 + \kappa_3\|\operatorname{div}\boldsymbol{v}\|_{0,\Omega}^2.
\end{aligned}
$$

Next, employing the inequality $ab \leqslant a^2 + \frac{1}{4}b^2$, we find that

$$
\kappa_1\sigma|\eta|_{1,\Omega}\|\boldsymbol{v}\|_{0,\Omega} \leqslant \kappa_1^2\sigma|\eta|_{1,\Omega}^2 + \frac{\sigma}{4}\|\boldsymbol{v}\|_{0,\Omega}^2 \quad \text{and} \quad \kappa_2\sigma\|\boldsymbol{v}\|_{0,\Omega}|q|_{1,\Omega} \leqslant \kappa_2^2\sigma|q|_{1,\Omega}^2 + \frac{\sigma}{4}\|\boldsymbol{v}\|_{0,\Omega}^2\,,
$$

which, together with the previous inequality, yields

$$
\begin{aligned}
\mathcal{A}(\vec{v}, \vec{v}) &\geqslant \frac{\sigma}{2}\|\boldsymbol{v}\|_{0,\Omega}^2 + \nu\|\eta\|_{0,\Omega}^2 - \kappa_1^2\sigma|\eta|_{1,\Omega}^2 + \kappa_1\nu|\eta|_{1,\Omega}^2 - \kappa_2^2\sigma|q|_{1,\Omega}^2 + \kappa_2|q|_{1,\Omega}^2 + \kappa_3\|\operatorname{div}\boldsymbol{v}\|_{0,\Omega}^2 \\
&\geqslant \min\left\{\frac{\sigma}{2}, \kappa_3\right\}\|\boldsymbol{v}\|_{\operatorname{div},\Omega}^2 + \nu\|\eta\|_{0,\Omega}^2 + \kappa_1(\nu - \kappa_1\sigma)|\eta|_{1,\Omega}^2 + \kappa_2(1 - \kappa_2\sigma)|q|_{1,\Omega}^2\,.
\end{aligned}
$$

Finally, the proof is completed by straightforward applications of the Poincaré inequality. □

We are now in a position to state the main result of this section, which yields the solvability of the continuous formulation (2.3).

Theorem 2.3
Assume the same hypotheses of Lemma 2.2. Then, formulation (2.3) admits a unique solution $\vec{u} := (\boldsymbol{u}, \omega, p) \in \mathbb{H}$. Moreover, there exists $C > 0$ such that

$$
\|\vec{u}\|_{\mathbb{H}} \leqslant C \left\{ \|\boldsymbol{a} \cdot \boldsymbol{t}\|_{-1/2,\Sigma} + \|\boldsymbol{f}\|_{0,\Omega} \right\}\,.
$$

Proof
The bilinear form $\mathcal{A}$ and the linear functional $\mathcal{G}$ are continuous (cf. (2.6)). Hence, the proof is a simple consequence of Lemma 2.2 and the well-known Lax–Milgram theorem. □

Notice that the unique solution of (2.1) is certainly the solution of (2.3), and hence, because the latter is also uniquely solvable, it is clear that the solutions of both problems coincide. This means,

in particular, that Theorem 2.1 is obviously valid for the solution $\vec{u} := (u, \omega, p)$ of (2.3) as well. This fact is employed later on in Section 4 to prove the efficiency of the proposed a posteriori error estimators.

3. THE AUGMENTED FINITE ELEMENT SCHEME

Let $\mathcal{T}_h$ be a regular family of triangulations of the polygonal region $\bar{\Omega}$ by triangles T of diameter h_T with mesh size $h := \max\{h_T : T \in \mathcal{T}_h\}$ and such that there holds $\bar{\Omega} = \cup\{T : T \in \mathcal{T}_h\}$. In addition, given an integer $k \geqslant 0$ and a subset S of $\mathbb{R}^2$, we denote by $P_k(S)$ the space of polynomials in two variables defined in S of total degree at most k, and we write $\mathbf{P}_k(S) = [P_k(S)]^2$. By $\mathbf{RT}_k(T)$, we will denote the local Raviart–Thomas space of order k defined as usual

$$\mathbf{RT}_k(T) := \mathbf{P}_k(T) \oplus P_k(T)\boldsymbol{x},$$

with $\boldsymbol{x}$ being a generic vector of $\mathbb{R}^2$. In addition, we let $\mathbf{RT}_k(\Omega)$ be the global Raviart–Thomas space of order k, that is,

$$\mathbf{RT}_k(\Omega) := \{\boldsymbol{v}_h \in \mathbf{H}(\text{div}; \Omega) : \quad \boldsymbol{v}_h|_T \in \mathbf{RT}_k(T) \quad \forall T \in \mathcal{T}_h\}. \tag{3.1}$$

Now, given finite element subspaces $\mathbf{H}_h^{\boldsymbol{u}} \subset \mathbf{H}_\Gamma(\text{div}; \Omega)$, $\mathrm{H}_h^\omega \subset \mathrm{H}_\Gamma^1(\Omega)$, and $\mathrm{H}_h^p \subset \mathrm{H}_\Sigma^1(\Omega)$, the Galerkin scheme associated with the continuous variational formulation (2.3) reads as follows: find $\vec{u}_h := (u_h, \omega_h, p_h) \in \mathbb{H}_h$ such that

$$\mathcal{A}(\vec{u}_h, \vec{v}_h) = \mathcal{G}(\vec{v}_h) \qquad \forall \vec{v}_h := (v_h, \eta_h, q_h) \in \mathbb{H}_h, \tag{3.2}$$

where the space $\mathbb{H}_h := \mathbf{H}_h^{\boldsymbol{u}} \times \mathrm{H}_h^\omega \times \mathrm{H}_h^p$, and κ_1, κ_2, and κ_3 are the same parameters employed in the continuous formulation (2.3).

Because the bilinear form $\mathcal{A}$ is bounded and strongly coercive on the whole space $\mathbb{H}$ (Theorem 2.3), the well-posedness of (3.2) is guaranteed with any arbitrary choice of the subspace $\mathbb{H}_h$. In particular, we define the following finite element subspaces for $k \geqslant 0$:

$$\mathbf{H}_h^{\boldsymbol{u}} := \mathbf{H}_\Gamma(\text{div}; \Omega) \cap \mathbf{RT}_k(\Omega) = \{\boldsymbol{v}_h \in \mathbf{H}_\Gamma(\text{div}; \Omega) : \quad \boldsymbol{v}_h|_T \in \mathbf{RT}_k(T) \quad \forall T \in \mathcal{T}_h\}, \tag{3.3}$$

$$\tilde{\mathbf{H}}_h^{\boldsymbol{u}} := \{\boldsymbol{v}_h \in \mathbf{H}_\Gamma(\text{div}; \Omega) : \quad \boldsymbol{v}_h|_T \in \mathbf{P}_{k+1}(T) \quad \forall T \in \mathcal{T}_h\}, \tag{3.4}$$

$$\mathrm{H}_h^\omega := \{\eta_h \in \mathrm{H}_\Gamma^1(\Omega) : \quad \eta_h|_T \in P_{k+1}(T) \quad \forall T \in \mathcal{T}_h\}, \tag{3.5}$$

$$\mathrm{H}_h^p := \{q_h \in \mathrm{H}_\Sigma^1(\Omega) : \quad q_h|_T \in P_{k+1}(T) \quad \forall T \in \mathcal{T}_h\}. \tag{3.6}$$

Notice that $\tilde{\mathbf{H}}_h^{\boldsymbol{u}}$ is the component of the Brezzi–Douglas–Marini finite element space approximating $\boldsymbol{u}$. According to the aforementioned assertion, we may consider the following families of finite elements: $\mathbb{H}_h := \mathbf{H}_h^{\boldsymbol{u}} \times \mathrm{H}_h^\omega \times \mathrm{H}_h^p$ or $\mathbb{H}_h := \tilde{\mathbf{H}}_h^{\boldsymbol{u}} \times \mathrm{H}_h^\omega \times \mathrm{H}_h^p$.

In general, we have the following main result, which establishes the unique solvability, and some convergence properties of the discrete problem (3.2).

Theorem 3.1
Assume that $\kappa_1 \in \left(0, \frac{\nu}{\sigma}\right)$, $\kappa_2 \in \left(0, \frac{1}{\sigma}\right)$, and $\kappa_3 > 0$, and let $\mathbb{H}_h$ be any finite element subspace of $\mathbb{H}$. Then, the discrete formulation (3.2) admits a unique solution $\vec{u}_h \in \mathbb{H}_h$. Moreover, there exist $\widehat{C}$ and $\tilde{C} > 0$ such that

$$\|\vec{u}_h\|_{\mathbb{H}} \leqslant \widehat{C} \left\{\|\boldsymbol{a} \cdot \boldsymbol{t}\|_{-1/2, \Sigma} + \|\boldsymbol{f}\|_{0, \Omega}\right\},$$

and

$$\|\vec{u} - \vec{u}_h\|_{\mathbb{H}} \leqslant \tilde{C} \inf_{\vec{v}_h \in \mathbb{H}_h} \|\vec{u} - \vec{v}_h\|_{\mathbb{H}}. \tag{3.7}$$

Proof
It follows straightforwardly from Lemma 2.2, Lax–Milgram theorem, and the Céa estimate. □

As usual, the estimate (3.7) and the approximation properties of the subspaces considered are the key ingredients to obtain the corresponding rate of convergence of the finite element scheme (3.2). In fact, let us consider the family $\mathbb{H}_h := \mathbf{H}_h^{\boldsymbol{u}} \times \mathrm{H}_h^{\omega} \times \mathrm{H}_h^{p}$, with $\mathbf{H}_h^{\boldsymbol{u}}$, H_h^{ω}, and H_h^{p}, given in (3.3), (3.5), and (3.6), respectively. Hence, we have the following (cf. [20, 23, 35]):

$\left(\mathrm{AP}_h^{\boldsymbol{u}}\right)$: there exists $C > 0$, independent of h, such that for each $s \in (0, k+1]$ and for each $\boldsymbol{v} \in \mathbf{H}^s(\Omega) \cap \mathbf{H}_\Gamma(\mathrm{div}; \Omega)$ with $\mathrm{div}\,\boldsymbol{v} \in \mathrm{H}^s(\Omega)$, there holds

$$\inf_{\boldsymbol{v}_h \in \mathbf{H}_h^{\boldsymbol{u}}} \|\boldsymbol{v} - \boldsymbol{v}_h\|_{\mathrm{div},\Omega} \leqslant C\,h^s \{\|\boldsymbol{v}\|_{s,\Omega} + \|\mathrm{div}\,\boldsymbol{v}\|_{s,\Omega}\}\,.$$

$\left(\mathrm{AP}_h^{\omega}\right)$: there exists $C > 0$, independent of h, such that for each $s \in (0, k+1]$ and for each $\eta \in \mathrm{H}^{s+1}(\Omega)$, there holds

$$\inf_{\eta_h \in \mathrm{H}_h^{\omega}} \|\eta - \eta_h\|_{1,\Omega} \leqslant C\,h^s \|\eta\|_{s+1,\Omega}\,.$$

$\left(\mathrm{AP}_h^{p}\right)$: there exists $C > 0$, independent of h, such that for each $s \in (0, k+1]$ and for each $q \in \mathrm{H}^{s+1}(\Omega)$, there holds

$$\inf_{q_h \in \mathrm{H}_h^{p}} \|q - q_h\|_{1,\Omega} \leqslant C\,h^s \|q\|_{s+1,\Omega}\,.$$

The following theorem provides the rate of convergence of our finite element scheme (3.2).

Theorem 3.2
Let k be a nonnegative integer, and let $\mathbf{H}_h^{\boldsymbol{u}}$, H_h^{ω}, and H_h^{p} be given by (3.3), (3.5), and (3.6). Let $\vec{\boldsymbol{u}} := (\boldsymbol{u}, \omega, p) \in \mathbb{H}$ and $\vec{\boldsymbol{u}}_h := (\boldsymbol{u}_h, \omega_h, p_h) \in \mathbb{H}_h := \mathbf{H}_h^{\boldsymbol{u}} \times \mathrm{H}_h^{\omega} \times \mathrm{H}_h^{p}$ be the unique solutions to the continuous and discrete problems (2.3) and (3.2), respectively. Assume that $\boldsymbol{u} \in \mathbf{H}^s(\Omega)$, $\mathrm{div}\,\boldsymbol{u} \in \mathrm{H}^s(\Omega)$, $\omega \in \mathrm{H}^{1+s}(\Omega)$, and $p \in \mathrm{H}^{1+s}(\Omega)$, for some $s \in (0, k+1]$. Then, there exists $\widehat{C} > 0$ independent of h such that

$$\|\vec{\boldsymbol{u}} - \vec{\boldsymbol{u}}_h\|_{\mathbb{H}} \leqslant \widehat{C}\,h^s \{\|\boldsymbol{u}\|_{s,\Omega} + \|\mathrm{div}\,\boldsymbol{u}\|_{s,\Omega} + \|\omega\|_{1+s,\Omega} + \|p\|_{1+s,\Omega}\}\,.$$

Proof
The proof follows from (3.7) and the approximation properties $\left(\mathrm{AP}_h^{\boldsymbol{u}}\right)$, $\left(\mathrm{AP}_h^{\omega}\right)$, and $\left(\mathrm{AP}_h^{p}\right)$. □

We remark here that if we consider $\mathbb{H}_h := \tilde{\mathbf{H}}_h^{\boldsymbol{u}} \times \mathrm{H}_h^{\omega} \times \mathrm{H}_h^{p}$, with $\tilde{\mathbf{H}}_h^{\boldsymbol{u}}$, H_h^{ω}, and H_h^{p}, given in (3.4)–(3.6), respectively, to solve problem (3.2), then the analogue of Theorem 3.2 does hold as well.

On the other hand, concerning the practical choice of the stabilization parameters κ_i, $i \in \{1, 2, 3\}$, particularly for the sake of the computational implementation of the augmented mixed finite element method, we first observe that the optimal values of κ_1 and κ_2, namely those yielding the largest ellipticity constant α (cf. Lemma 2.2), are given by the midpoints of the corresponding feasible intervals, that is, $\kappa_1 = \frac{\nu}{2\sigma}$ and $\kappa_2 = \frac{1}{2\sigma}$. In addition, as suggested by the first term in the last inequality of the proof of Lemma 2.2, a suitable choice for κ_3 would be given by any value $\geqslant \frac{\sigma}{2}$. The selections described here are employed later on in Section 5.

4. A POSTERIORI ERROR ANALYSIS

Let $\mathcal{E}_h$ be the set of all edges of the triangulation $\mathcal{T}_h$, and given $T \in \mathcal{T}_h$, we let $\mathcal{E}(T)$ be the set of its edges. Then we write $\mathcal{E}_h = \mathcal{E}_h(\Omega) \cup \mathcal{E}_h(\Gamma) \cup \mathcal{E}_h(\Sigma)$, where $\mathcal{E}_h(\Omega) := \{e \in \mathcal{E}_h : e \subseteq \Omega\}$, $\mathcal{E}_h(\Gamma) := \{e \in \mathcal{E}_h : e \subseteq \Gamma\}$, and analogously for $\mathcal{E}_h(\Sigma)$. In what follows, h_e stands for the length of a given edge e. Also, for each edge $e \in \mathcal{E}_h$, we fix a unit normal vector $\boldsymbol{n}_e := (n_1, n_2)^{\mathrm{t}}$ and let $\boldsymbol{t}_e := (-n_2, n_1)^{\mathrm{t}}$ be the corresponding fixed unit tangential vector along e. However, when no confusion arises, we simply write $\boldsymbol{n}$ and $\boldsymbol{t}$ instead of $\boldsymbol{n}_e$ and $\boldsymbol{t}_e$, respectively. Now, let $\boldsymbol{v} \in \mathbf{L}^2(\Omega)$

such that $\mathbf{v}|_T \in \mathbf{C}(T)$ on each $T \in \mathcal{T}_h$. Then, given $T \in \mathcal{T}_h$ and $e \in \mathcal{E}(T) \cap \mathcal{E}_h(\Omega)$, we denote by $[\mathbf{v} \cdot \mathbf{t}]$ and $[\mathbf{v} \cdot \mathbf{n}]$ the tangential and normal jumps of $\mathbf{v}$ across e, that is, $[\mathbf{v} \cdot \mathbf{t}] := (\mathbf{v}|_T - \mathbf{v}|_{T'})|_e \cdot \mathbf{t}$ and $[\mathbf{v} \cdot \mathbf{n}] := (\mathbf{v}|_T - \mathbf{v}|_{T'})|_e \cdot \mathbf{n}$, where T and T' are the triangles of $\mathcal{T}_h$ having e as a common edge.

4.1. The main results

As in the previous sections, we consider $\mathbb{H}_h = \mathbf{H}_h^{\mathbf{u}} \times \mathrm{H}_h^\omega \times \mathrm{H}_h^p$, where, given an integer $k \geq 0$, the component subspaces are defined by (3.3), (3.5), and (3.6), respectively. Next, letting $\vec{\mathbf{u}}_h := (\mathbf{u}_h, \omega_h, p_h) \in \mathbb{H}_h$ be the unique solution of (3.2), we set the residuals

$$\mathbf{r}(\mathbf{u}_h, \omega_h) := \mathbf{f} - \sigma \mathbf{u}_h - \nu \operatorname{curl} \omega_h, \quad \mathbf{r}(\mathbf{u}_h, p_h) := \mathbf{f} - \sigma \mathbf{u}_h - \nabla p_h,$$

$$\mathbf{r}(\mathbf{u}_h, \omega_h, p_h) := r(\mathbf{u}_h, \omega_h) - \nabla p_h,$$

and define for each $T \in \mathcal{T}_h$ the a posteriori error indicators

$$\theta_T^2 := \|\mathbf{r}(\mathbf{u}_h, \omega_h, p_h)\|_{0,T}^2 + \|\operatorname{div} \mathbf{u}_h\|_{0,T}^2 + h_T^2 \|\operatorname{rot} \mathbf{u}_h - \omega_h\|_{0,T}^2 + h_T^2 \|\operatorname{rot}\{\mathbf{r}(\mathbf{u}_h, \omega_h)\}\|_{0,T}^2$$

$$+ \sum_{e \in \mathcal{E}(T) \cap \mathcal{E}_h(\Sigma)} h_e \|\mathbf{a} \cdot \mathbf{t} - \mathbf{u}_h \cdot \mathbf{t}\|_{0,e}^2 + \sum_{e \in \mathcal{E}(T) \cap \mathcal{E}_h(\Omega)} h_e \|[\mathbf{u}_h \cdot \mathbf{t}]\|_{0,e}^2 \tag{4.1}$$

$$+ \sum_{e \in \mathcal{E}(T) \cap \mathcal{E}_h(\Omega)} h_e \|[\mathbf{r}(\mathbf{u}_h, \omega_h) \cdot \mathbf{t}]\|_{0,e}^2 + \sum_{e \in \mathcal{E}(T) \cap \mathcal{E}_h(\Sigma)} h_e \|\mathbf{r}(\mathbf{u}_h, \omega_h) \cdot \mathbf{t}\|_{0,e}^2,$$

and

$$\vartheta_T^2 := \theta_T^2 + h_T^2 \|\operatorname{div}\{\mathbf{r}(\mathbf{u}_h, p_h)\}\|_{0,T}^2 + \sum_{e \in \mathcal{E}(T) \cap \mathcal{E}_h(\Omega)} h_e \|[\mathbf{r}(\mathbf{u}_h, p_h) \cdot \mathbf{n}]\|_{0,e}^2$$

$$+ \sum_{e \in \mathcal{E}(T) \cap \mathcal{E}_h(\Gamma)} h_e \|\mathbf{r}(\mathbf{u}_h, p_h) \cdot \mathbf{n}\|_{0,e}^2, \tag{4.2}$$

so that the global a posteriori error estimators are given, respectively, by

$$\theta := \left\{ \sum_{T \in \mathcal{T}_h} \theta_T^2 \right\}^{1/2} \quad \text{and} \quad \vartheta := \left\{ \sum_{T \in \mathcal{T}_h} \vartheta_T^2 \right\}^{1/2}. \tag{4.3}$$

The following theorems constitute the main results of this section.

Theorem 4.1
Assume that $\mathbf{f}$ is piecewise polynomial, and let $\vec{\mathbf{u}} := (\mathbf{u}, \omega, p) \in \mathbb{H}$ and $\vec{\mathbf{u}}_h := (\mathbf{u}_h, \omega_h, p_h) \in \mathbb{H}_h$ be the unique solutions of (2.3) and (3.2), respectively. Then, there exist constants $C_{\text{rel}} > 0$ and $C_{\text{eff}} > 0$, independent of h, such that

$$C_{\text{eff}} \, \theta \leq \|\vec{\mathbf{u}} - \vec{\mathbf{u}}_h\|_{\mathbb{H}} \leq C_{\text{rel}} \, \theta. \tag{4.4}$$

Theorem 4.2
Assume that $\mathbf{f}$ is piecewise polynomial, and let $\vec{\mathbf{u}} := (\mathbf{u}, \omega, p) \in \mathbb{H}$ and $\vec{\mathbf{u}}_h := (\mathbf{u}_h, \omega_h, p_h) \in \mathbb{H}_h$ be the unique solutions of (2.3) and (3.2), respectively. Then, there exist constants $c_{\text{rel}} > 0$ and $c_{\text{eff}} > 0$, independent of h, such that

$$c_{\text{eff}} \, \vartheta \leq \|\vec{\mathbf{u}} - \vec{\mathbf{u}}_h\|_{\mathbb{H}} \leq c_{\text{rel}} \, \vartheta. \tag{4.5}$$

We remark that when $\mathbf{f}$ is not piecewise polynomial, then high-order terms arising from suitable polynomial approximations of this function will appear in (4.4) and (4.5). The upper and lower bounds in these inequalities are known as the reliability and efficiency estimates, respectively, and they are derived later on in Sections 4.2 and 4.3. Note, however, that the inequalities (4.4) and (4.5), together with the fact that $\theta \leq \vartheta$, imply that the sharper a posterior error estimate is actually given by

$$c_{\text{eff}}\, \vartheta \ \leqslant \ \| \, \vec{u} \, - \, \vec{u}_h \, \|_{\mathbb{H}} \ \leqslant \ C_{\text{rel}}\, \theta \, .$$

Throughout the rest of this section, we employ the Clément interpolation operator I_h, which maps $H^1(\Omega)$ onto X_h (cf. [36]), where

$$X_h \ := \ \big\{ \varphi_h \in C(\bar{\Omega}) : \quad \varphi_h|_T \, \in \, P_1(T) \quad \forall\, T \in \mathcal{T}_h \big\} \, .$$

In addition, the local approximation properties of I_h are summarized as follows.

Lemma 4.3
There exist c_1 and $c_2 > 0$, independent of h, such that for all $\varphi \in H^1(\Omega)$, there holds

$$\| \varphi - I_h(\varphi) \|_{0,T} \ \leqslant \ c_1 \, h_T \, \| \varphi \|_{1,\Delta(T)} \qquad \forall\, T \in \mathcal{T}_h$$

and

$$\| \varphi - I_h(\varphi) \|_{0,e} \ \leqslant \ c_2 \, h_e^{1/2} \, \| \varphi \|_{1,\Delta(e)} \qquad \forall\, e \in \mathcal{E}_h(\Omega) \cup \mathcal{E}_h(\Gamma) \, ,$$

where $\Delta(T) := \cup \{ T' \in \mathcal{T}_h : \quad T' \cap T \neq \emptyset \}$ and $\Delta(e) := \cup \{ T' \in \mathcal{T}_h : \quad T' \cap e \neq \emptyset \}$.

Proof
See [36]. □

4.2. Reliability of the a posteriori error estimators

We first deduce from the $\mathbb{H}$-ellipticity of $\mathcal{A}$ (cf. Lemma (2.2)) that there holds the global inf-sup condition

$$\alpha \, \| \vec{w} \|_{\mathbb{H}} \ \leqslant \ \sup_{\substack{\vec{v} \in \mathbb{H} \\ \vec{v} \neq \mathbf{0}}} \frac{\mathcal{A}(\vec{w}, \vec{v})}{\| \vec{v} \|_{\mathbb{H}}} \qquad \forall\, \vec{w} := (\mathbf{w}, \chi, r) \in \mathbb{H} \, . \tag{4.6}$$

Hence, we have the following preliminary estimate for the error.

Lemma 4.4
Let $\vec{u} := (\mathbf{u}, \omega, p) \in \mathbb{H}$ and $\vec{u}_h := (\mathbf{u}_h, \omega_h, p_h) \in \mathbb{H}_h$ be the unique solutions of (2.3) and (3.2), respectively. Then, there exists a constant $c > 0$, independent of h, such that

$$\| \vec{u} - \vec{u}_h \|_{\mathbb{H}} \ \leqslant \ C \, \| \, E \, \|_{\mathbb{H}'} \, ,$$

where

$$E(\vec{v}) \ := \ E_1(\mathbf{v}) + E_2(\eta) + E_3(q) \qquad \forall\, \vec{v} := (\mathbf{v}, \eta, q) \in \mathbb{H} \, ,$$

and $E_1 : \mathbf{H}_\Gamma(\text{div}; \Omega) \to \mathbb{R}$, $E_2 : H^1_\Gamma(\Omega) \to \mathbb{R}$, and $E_3 : H^1_\Sigma(\Omega) \to \mathbb{R}$ are the linear and bounded functionals defined by

$$E_1(\mathbf{v}) \ := \ \int_\Omega \mathbf{r}(\mathbf{u}_h, \omega_h) \cdot \mathbf{v} + \int_\Omega p_h \, \text{div}\, \mathbf{v} - k_3 \int_\Omega \text{div}\, \mathbf{u}_h \, \text{div}\, \mathbf{v} \quad \forall\, \mathbf{v} \in \mathbf{H}_\Gamma(\text{div}; \Omega) \, , \tag{4.7}$$

$$E_2(\eta) \ := \ \nu \, \langle \mathbf{a} \cdot \mathbf{t}, \eta \rangle_\Sigma - \nu \int_\Omega \omega_h \, \eta + \nu \int_\Omega \mathbf{u}_h \cdot \text{curl}\, \eta + k_1 \int_\Omega \mathbf{r}(\mathbf{u}_h, \omega_h) \cdot \text{curl}\, \eta \, , \tag{4.8}$$

for all $\eta \in H^1_\Gamma(\Omega)$, and

$$E_3(q) \ := \ k_2 \int_\Omega \mathbf{r}(\mathbf{u}_h, p_h) \cdot \nabla q \quad - \int_\Omega q \, \text{div}\, \mathbf{u}_h \qquad \forall\, q \in H^1_\Sigma(\Omega) \, . \tag{4.9}$$

In addition, there holds

$$E(\vec{v}_h) \ = \ 0 \qquad \forall\, \vec{v}_h := (\mathbf{v}_h, \eta_h, q_h) \in \mathbb{H}_h \, . \tag{4.10}$$

Proof
Applying (4.6) to the error $\vec{w} := \vec{u} - \vec{u}_h$ and then employing (2.3) and the definitions of $\mathcal{A}$ and $\mathcal{G}$ (cf. (2.4) and (2.5)), we arrive at

$$\alpha \|\vec{u} - \vec{u}_h\|_{\mathbb{H}} \leqslant \sup_{\substack{\vec{v} \in \mathbb{H} \\ \vec{v} \neq 0}} \frac{\mathcal{G}(\vec{v}) - \mathcal{A}(\vec{u}_h, \vec{v})}{\|\vec{v}\|_{\mathbb{H}}} := \|\mathcal{G} - \mathcal{A}(\vec{u}_h, \cdot)\|_{\mathbb{H}'},$$

where, bearing in mind (4.7)–(4.9), there holds

$$\mathcal{G}(\vec{v}) - \mathcal{A}(\vec{u}_h, \vec{v}) = E_1(v) + E_2(\eta) + E_3(q) \qquad \forall \vec{v} := (v, \eta, q) \in \mathbb{H}.$$

Moreover, it is straightforward from (3.2) that $\mathcal{G}(\vec{v}_h) - \mathcal{A}(\vec{u}_h, \vec{v}_h) = 0 \quad \forall \vec{v}_h := (v_h, \eta_h, q_h) \in \mathbb{H}_h$, which, denoting $E := \mathcal{G} - \mathcal{A}(\vec{u}_h, \cdot)$, gives (4.10) and ends the proof. $\qquad \square$

In order to complete the derivation of the a posteriori error estimates, we need to obtain a suitable upper bound for $\|E\|_{\mathbb{H}'}$. This is performed in the subsequent sections.

4.2.1. Reliability of θ. We use once the Clément interpolation operator I_h. More precisely, given $\vec{v} := (v, \eta, q) \in \mathbb{H}$, we let $\vec{v}_h := (\mathbf{0}, I_h(\eta), 0) \in \mathbb{H}_h$, so that, using (4.10), we find that

$$E(\vec{v}) = E_1(v) + E_2(\eta - I_h(\eta)) + E_3(q). \tag{4.11}$$

Note here that the fact that I_h preserves Dirichlet boundary conditions (cf. [36]) ensures that $I_h(\eta)$ also vanishes on Γ.

Furthermore, it is easy to see that

$$E_2(\eta - I_h(\eta)) = E_{21}(\eta - I_h(\eta)) + E_{22}(\eta - I_h(\eta)), \tag{4.12}$$

where E_{21} and E_{22} are defined as

$$E_{21}(\eta - I_h(\eta)) := \nu \langle \mathbf{a} \cdot \mathbf{t}, \eta - \eta_h \rangle_\Sigma - \nu \int_\Omega \omega_h(\eta - \eta_h) + \nu \int_\Omega \mathbf{u}_h \cdot \mathrm{curl}(\eta - \eta_h), \tag{4.13}$$

and

$$E_{22}(\eta - I_h(\eta)) := k_1 \int_\Omega \mathbf{r}(\mathbf{u}_h, \omega_h) \cdot \mathrm{curl}(\eta - \eta_h). \tag{4.14}$$

Consequently, in order to estimate $|E(\vec{v})|$ in terms of residual terms and $\|\vec{v}\|_{\mathbb{H}}$, thus deriving a suitable bound for $\|E\|_{\mathbb{H}'}$, we now proceed to obtain upper bounds for each one of the aforementioned components.

Lemma 4.5
There exists $C > 0$, independent of h, such that

$$|E_1(v)| + |E_3(q)| \leqslant C \left\{ \sum_{T \in \mathcal{T}_h} \widetilde{\theta}_T^2 \right\}^{1/2} \|\vec{v}\|_{\mathbb{H}} \qquad \forall \vec{v} := (v, \eta, q) \in \mathbb{H},$$

where

$$\widetilde{\theta}_T^2 := \big\| \mathbf{r}(\mathbf{u}_h, \omega_h, p_h) \big\|_{0,T}^2 + \big\| \mathrm{div}\, \mathbf{u}_h \big\|_{0,T}^2 \qquad \forall T \in \mathcal{T}_h.$$

Proof
Let $\vec{v} := (v, \eta, q) \in \mathbb{H}$. Integrating by parts in Ω and using that $p_h = 0$ on Σ and that $\mathbf{v} \cdot \mathbf{n} = 0$ on Γ, we obtain

$$\int_\Omega p_h \,\mathrm{div}\, \mathbf{v} = -\int_\Omega \nabla p_h \cdot \mathbf{v},$$

which, according to (4.7), yields

$$E_1(\boldsymbol{v}) = \int_\Omega \mathbf{r}(\boldsymbol{u}_h, \omega_h, p_h) \cdot \boldsymbol{v} - k_3 \int_\Omega \operatorname{div} \boldsymbol{u}_h \operatorname{div} \boldsymbol{v}. \tag{4.15}$$

In turn, integrating by parts again in Ω and using now that $\nabla q \cdot \boldsymbol{t} = 0$ on Σ (because q vanishes there), $\omega_h = 0$ on Γ, and certainly rot $\nabla q = 0$, we find that

$$\int_\Omega \operatorname{curl} \omega_h \cdot \nabla q = 0,$$

which implies, together with (4.9), that

$$E_3(q) := k_2 \int_\Omega \mathbf{r}(\boldsymbol{u}_h, \omega_h, p_h) \cdot \nabla q \quad - \int_\Omega q \operatorname{div} \boldsymbol{u}_h. \tag{4.16}$$

Hence, the proof follows from straightforward applications of the Cauchy–Schwarz inequality in (4.15) and (4.16). □

Lemma 4.6
There exists $C > 0$, independent of h, such that

$$|E_{21}(\eta - I_h(\eta))| \leqslant C \left\{ \sum_{T \in \mathcal{T}_h} \hat{\theta}_T^2 \right\}^{1/2} \|\vec{\boldsymbol{v}}\|_{\mathbb{H}} \qquad \forall \, \vec{\boldsymbol{v}} := (\boldsymbol{v}, \eta, q) \in \mathbb{H},$$

where

$$\widehat{\theta}_T^2 := h_T^2 \, \| \operatorname{rot} \boldsymbol{u}_h - \omega_h \|_{0,T}^2 + \sum_{e \in \mathcal{E}(T) \cap \mathcal{E}_h(\Omega)} h_e \, \| [\boldsymbol{u}_h \cdot \boldsymbol{t}] \|_{0,e}^2 + \sum_{e \in \mathcal{E}(T) \cap \mathcal{E}_h(\Sigma)} h_e \, \| \boldsymbol{a} \cdot \boldsymbol{t} - \boldsymbol{u}_h \cdot \boldsymbol{t} \|_{0,e}^2.$$

Proof
We begin by looking at the third term defining E_{21} (cf. (4.13)). In fact, integrating by parts in each $T \in \mathcal{T}_h$, we obtain

$$\int_\Omega \boldsymbol{u}_h \cdot \operatorname{curl}(\eta - I_h(\eta)) = \sum_{T \in \mathcal{T}_h} \left\{ \int_T \operatorname{rot} \boldsymbol{u}_h \, (\eta - I_h(\eta)) - \int_{\partial T} \boldsymbol{u}_h \cdot \boldsymbol{t} \, (\eta - I_h(\eta)) \right\},$$

which, using that $\eta = I_h(\eta) = 0$ on Γ, yields

$$\int_\Omega \boldsymbol{u}_h \cdot \operatorname{curl}(\eta - I_h(\eta)) = \sum_{T \in \mathcal{T}_h} \int_T \operatorname{rot} \boldsymbol{u}_h \, (\eta - I_h(\eta)) - \sum_{e \in \mathcal{E}_h(\Omega)} \int_e [\boldsymbol{u}_h \cdot \boldsymbol{t}] \, (\eta - I_h(\eta))$$

$$- \sum_{e \in \mathcal{E}_h(\Sigma)} \int_e \boldsymbol{u}_h \cdot \boldsymbol{t} \, (\eta - I_h(\eta)).$$

It follows from (4.13) and the foregoing equality that

$$E_{21}(\eta - I_h(\eta)) = \nu \sum_{T \in \mathcal{T}_h} \int_T \{\operatorname{rot} \boldsymbol{u}_h - \omega_h\} \, (\eta - I_h(\eta)) - \nu \sum_{e \in \mathcal{E}_h(\Omega)} \int_e [\boldsymbol{u}_h \cdot \boldsymbol{t}] \, (\eta - I_h(\eta))$$

$$+ \nu \sum_{e \in \mathcal{E}_h(\Sigma)} \int_e \{\boldsymbol{a} \cdot \boldsymbol{t} - \boldsymbol{u}_h \cdot \boldsymbol{t}\} \, (\eta - I_h(\eta)),$$

and hence, the proof is completed by applying Cauchy–Schwarz inequality, the approximation properties of the Clément interpolant I_h (cf. Lemma 4.3), and the fact that the number of triangles of $\Delta(T)$ and $\Delta(e)$ is bounded independently of $T \in \mathcal{T}_h$ and $e \in \mathcal{E}_h$, respectively. □

Lemma 4.7
There exists $C > 0$, independent of h, such that

$$|E_{22}(\eta - I_h(\eta))| \leqslant C \left\{ \sum_{T \in \mathcal{T}_h} \hat{\theta}_T^2 \right\}^{1/2} \|\vec{v}\|_{\mathbb{H}} \qquad \forall \, \vec{v} := (v, \eta, q) \in \mathbb{H},$$

where

$$\hat{\theta}_T^2 := h_T^2 \left\| \operatorname{rot}\{\mathbf{r}(u_h, \omega_h)\} \right\|_{0,T}^2 + \sum_{e \in \mathcal{E}(T) \cap \mathcal{E}_h(\Omega)} h_e \left\| [\mathbf{r}(u_h, \omega_h) \cdot t] \right\|_{0,e}^2$$

$$+ \sum_{e \in \mathcal{E}(T) \cap \mathcal{E}_h(\Sigma)} h_e \left\| \mathbf{r}(u_h, \omega_h) \cdot t \right\|_{0,e}^2.$$

Proof
It follows from (4.14), integrating by parts in each $T \in \mathcal{T}_h$, that

$$E_{22}(\eta - I_h(\eta)) = k_1 \sum_{T \in \mathcal{T}_h} \left\{ \int_T (\eta - I_h(\eta)) \operatorname{rot}\{\mathbf{r}(u_h, \omega_h)\} - \int_{\partial T} (\eta - I_h(\eta)) \mathbf{r}(u_h, \omega_h) \cdot t \right\},$$

which, using that $\eta = I_h(\eta) = 0$ on Γ, yields

$$E_{22}(\eta - I_h(\eta)) = k_1 \sum_{T \in \mathcal{T}_h} \int_T (\eta - I_h(\eta)) \operatorname{rot}\{\mathbf{r}(u_h, \omega_h)\}$$

$$- k_1 \sum_{e \in \mathcal{E}_h(\Omega)} \int_e (\eta - I_h(\eta)) [\mathbf{r}(u_h, \omega_h) \cdot t] - k_1 \sum_{e \in \mathcal{E}_h(\Sigma)} \int_e (\eta - I_h(\eta)) \mathbf{r}(u_h, \omega_h) \cdot t.$$

In this way, proceeding as in the previous proof, that is, applying Cauchy–Schwarz inequality, the approximation properties of I_h, and the uniform boundedness of the number of triangles of $\Delta(T)$ and $\Delta(e)$, the proof is concluded. □

We end this section by remarking that the reliability estimate for $\boldsymbol{\theta}$ (cf. upper estimate in (4.4), Theorem 4.1) follows from identities (4.11)–(4.14), together with Lemmata 4.4–4.7.

4.2.2. Reliability of $\boldsymbol{\vartheta}$. This estimate follows by bounding $\|E\|_{\mathbb{H}'}$ (cf. Lemma 4.4) after using twice the Clément interpolant I_h. More precisely, given $\vec{v} := (v, \eta, q) \in \mathbb{H}$, we now let

$$\vec{v}_h := (0, I_h(\eta), I_h(q)) \in \mathbb{H}_h,$$

so that, using (4.10), we find that

$$E(\vec{v}) = E_1(v) + E_2(\eta - I_h(\eta)) + E_3(q - I_h(q)), \qquad (4.17)$$

where $E_1(v)$ and $E_2(\eta - I_h(\eta))$ are given by (4.7) and (4.12)–(4.14), respectively, and

$$E_3(q - I_h(q)) := k_2 \int_\Omega \mathbf{r}(u_h, p_h) \cdot \nabla (q - I_h(q)) \quad - \int_\Omega (q - I_h(q)) \operatorname{div} u_h. \qquad (4.18)$$

Note here that the fact that I_h preserves Dirichlet boundary conditions (cf. [36]) ensures now that $I_h(\eta)$ and $I_h(q)$ also vanish on Γ and Σ, respectively.

Next, similarly as in Section 4.2.1, and in order to estimate $|E(\vec{v})|$ in terms of residual terms and $\|\vec{v}\|_{\mathbb{H}}$, thus deriving an alternative bound for $\|E\|_{\mathbb{H}'}$, we should obtain upper bounds for each one of the components in (4.17). Actually, because the estimates for $E_1(v)$ and $E_2(\eta - I_h(\eta))$ are

already available from Lemmata 4.5–4.7 and (4.12), we would just need to estimate the remaining third term. Nevertheless, it is much simpler to recall here that $\theta \leqslant \vartheta$, whence the reliability of ϑ follows obviously from that of θ.

4.3. Efficiency of the a posteriori error estimators

In this section, we show the efficiency of our a posteriori error estimators θ (cf. (4.1)) and ϑ (cf. (4.2)). Equivalently, we provide upper bounds depending on the actual errors for the eight terms defining the local indicator θ_T^2 and for the remaining three terms that complete the definition of ϑ. The easiest ones are the first two terms defining θ, for which, using from Theorem 2.1 that $f = \sigma u + \nu \operatorname{curl}\omega + \nabla p$ and $\operatorname{div} u = 0$ in Ω, we find that

$$\|\mathbf{r}(u_h, \omega_h, p_h)\|_{0,T}^2 = \left\| \{\sigma u + \nu \operatorname{curl}\omega + \nabla p\} - \sigma u_h - \nu \operatorname{curl}\omega_h - \nabla p_h \right\|_{0,T}^2 \tag{4.19}$$
$$\leqslant C \left\{ \|u - u_h\|_{0,T}^2 + |\omega - \omega_h|_{1,T}^2 + |p - p_h|_{1,T}^2 \right\},$$

where $C := \sigma^2 + \nu^2 + 1$, and

$$\|\operatorname{div} u_h\|_{0,T}^2 = \|\operatorname{div}(u_h - u)\|_{0,T}^2 \leqslant \|u - u_h\|_{\operatorname{div},\Omega}^2. \tag{4.20}$$

The derivation of the corresponding upper bounds for the remaining terms in (4.1) and (4.2) is performed next. To this end, we proceed as in [37] and [6] and apply the localization technique based on triangle-bubble and edge-bubble functions, together with extension operators and inverse inequalities. Therefore, we now introduce further notations and preliminary results. Given $T \in \mathcal{T}_h$ and $e \in \mathcal{E}(T)$, we let ψ_T and ψ_e be the usual triangle-bubble and edge-bubble functions, respectively ([38, Eqns (1.5) and (1.6)]), which satisfy

  i) $\psi_T \in P_3(T)$, $\psi_T = 0$ on ∂T, $\operatorname{supp}(\psi_T) \subseteq T$, and $0 \leqslant \psi_T \leqslant 1$ in T.
  ii) $\psi_e|_T \in P_2(T)$, $\psi_e = 0$ on $\partial T \setminus e$, $\operatorname{supp}(\psi_e) \subseteq w_e := \cup\{T' \in \mathcal{T}_h : e \in \mathcal{E}(T')\}$, and $0 \leqslant \psi_e \leqslant 1$ in w_e.

We also know from [39] that, given $k \in \mathbb{N} \cup \{0\}$, there exists an extension operator $L : C(e) \to C(T)$ that satisfies $L(p) \in P_k(T)$ and $L(p)|_e = p$ for all $p \in P_k(e)$. Additional properties of ψ_T, ψ_e, and L are collected in the following lemma.

Lemma 4.8
Given $k \in \mathbb{N} \cup \{0\}$, there exist positive constants c_1, c_2, and c_3, depending only on k and the shape regularity of the triangulations (minimum angle condition), such that for each $T \in \mathcal{T}_h$ and $e \in \mathcal{E}(T)$, there hold

$$\|q\|_{0,T}^2 \leqslant c_1 \|\psi_T^{1/2} q\|_{0,T}^2 \qquad \forall q \in P_k(T), \tag{4.21}$$

$$\|p\|_{0,e}^2 \leqslant c_2 \|\psi_e^{1/2} p\|_{0,e}^2 \qquad \forall p \in P_k(e), \tag{4.22}$$

$$\|\psi_e^{1/2} L(p)\|_{0,T}^2 \leqslant c_3 h_e \|p\|_{0,e}^2 \qquad \forall p \in P_k(e). \tag{4.23}$$

Proof
See [39, Lemma 4.1]. □

The following inverse inequality is also employed.

Lemma 4.9
Let $k, l, m \in \mathbb{N} \cup \{0\}$ such that $l \leqslant m$. Then there exists $c > 0$, depending only on k, l, m, and the shape regularity of the triangulations, such that for each $T \in \mathcal{T}_h$, there holds

$$|q|_{m,T} \leqslant c\, h_T^{l-m} |q|_{l,T} \qquad \forall q \in P_k(T). \tag{4.24}$$

Proof
See [35, Theorem 3.2.6]. □

We continue our efficiency analysis with the estimate for the third term defining (4.1).

Lemma 4.10
There exists $C > 0$, independent of h, such that

$$h_T^2 \, \| \operatorname{rot} \boldsymbol{u}_h \, - \, \omega_h \|_{0,T}^2 \; \leqslant \; C \, \left\{ \| \boldsymbol{u} - \boldsymbol{u}_h \|_{0,T}^2 \, + \, h_T^2 \, \| \omega - \omega_h \|_{0,T}^2 \right\} \qquad \forall \, T \in \mathcal{T}_h \,. \tag{4.25}$$

Proof
It is similar to the proof of [6, Lemma 20]. Given $T \in \mathcal{T}_h$, we denote $\gamma_T := \operatorname{rot} \boldsymbol{u}_h - \omega_h$ in T. Applying (4.21) to γ_T and then using from Theorem 2.1 that $\operatorname{rot} \boldsymbol{u} = \omega$ in Ω, we find that

$$\| \gamma_T \|_{0,T}^2 \; \leqslant \; c_1 \, \| \psi_T^{1/2} \gamma_T \|_{0,T}^2 \; = \; c_1 \int_T \psi_T \, \gamma_T \, \{ \operatorname{rot} \boldsymbol{u}_h \, - \, \omega_h \}$$

$$= \; - c_1 \int_T \psi_T \, \gamma_T \, \operatorname{rot}(\boldsymbol{u} - \boldsymbol{u}_h) \, + \, c_1 \int_T \psi_T \, \gamma_T \, (\omega - \omega_h) \,. \tag{4.26}$$

Next, integrating by parts in T and recalling that ψ_T vanishes on ∂T, we obtain

$$\int_T \psi_T \, \gamma_T \, \operatorname{rot}(\boldsymbol{u} - \boldsymbol{u}_h) \; = \; \int_T (\boldsymbol{u} - \boldsymbol{u}_h) \cdot \operatorname{curl}(\psi_T \, \gamma_T) \,,$$

which replacing back into (4.26) leads to

$$\| \gamma_T \|_{0,T}^2 \; \leqslant \; - c_1 \int_T (\boldsymbol{u} - \boldsymbol{u}_h) \cdot \operatorname{curl}(\psi_T \, \gamma_T) \, + \, c_1 \int_T \psi_T \, \gamma_T \, (\omega - \omega_h) \,. \tag{4.27}$$

Hence, applying the Cauchy–Schwarz inequality and the inverse estimate (4.24), we easily deduce from (4.27) that

$$\| \gamma_T \|_{0,T}^2 \; \leqslant \; C \, \| \psi_T \, \gamma_T \|_{0,T} \, \left\{ h_T^{-1} \, \| \boldsymbol{u} - \boldsymbol{u}_h \|_{0,T} \, + \, \| \omega - \omega_h \|_{0,T} \right\} \,,$$

which yields

$$h_T \, \| \gamma_T \|_{0,T} \; \leqslant \; C \, \left\{ \| \boldsymbol{u} - \boldsymbol{u}_h \|_{0,T} \, + \, h_T \, \| \omega - \omega_h \|_{0,T} \right\} \,,$$

thus implying (4.25) and completing the proof. □

We now aim to estimate the terms involving $\mathbf{r}(\boldsymbol{u}_h, \omega_h)$. The following lemma, whose proof makes use of Lemmas 4.8 and 4.9, will be employed for this purpose.

Lemma 4.11
Let $\boldsymbol{\rho}_h \in \mathbf{L}^2(\Omega)$ be a piecewise polynomial of degree $k \geqslant 0$ on each $T \in \mathcal{T}_h$, and let $\boldsymbol{\rho} \in \mathbf{L}^2(\Omega)$ be such that $\operatorname{rot} \{ \boldsymbol{\rho} \} = 0$ in Ω. Then, there exist c and $\widetilde{c} > 0$, independent of h, such that

$$h_T^2 \, \| \operatorname{rot} \{ \boldsymbol{\rho}_h \} \|_{0,T}^2 \; \leqslant \; c \, \| \boldsymbol{\rho} - \boldsymbol{\rho}_h \|_{0,T}^2 \qquad \forall \, T \in \mathcal{T}_h \,, \tag{4.28}$$

and

$$h_e \, \| [\boldsymbol{\rho}_h \cdot \boldsymbol{t}] \|_{0,e}^2 \; \leqslant \; \widetilde{c} \, \| \boldsymbol{\rho} - \boldsymbol{\rho}_h \|_{0,w_e}^2 \qquad \forall \, e \in \mathcal{E}_h(\Omega) \,. \tag{4.29}$$

Proof
For the proof of (4.28), we refer to [40, Lemma 4.3], whereas (4.29) is a slight modification of the proof of [40, Lemma 4.4]. We omit further details. □

As a straightforward consequence of the foregoing lemma, we have the following result.

Lemma 4.12
There exist C_1 and $C_2 > 0$, independent of h, such that

$$h_T^2 \, \| \operatorname{rot} \{ \mathbf{r}(\boldsymbol{u}_h, \omega_h) \} \|_{0,T}^2 \;\leqslant\; C_1 \, \{ \|\boldsymbol{u} - \boldsymbol{u}_h\|_{0,T}^2 \,+\, |\omega - \omega_h|_{1,T}^2 \} \qquad \forall \, T \in \mathcal{T}_h \,, \qquad (4.30)$$

and

$$h_e \, \| [\mathbf{r}(\boldsymbol{u}_h, \omega_h) \cdot \boldsymbol{t}] \|_{0,e}^2 \;\leqslant\; C_2 \, \{ \|\boldsymbol{u} - \boldsymbol{u}_h\|_{0,w_e}^2 \,+\, |\omega - \omega_h|_{1,w_e}^2 \} \qquad \forall \, e \in \mathcal{E}_h(\Omega) \,. \qquad (4.31)$$

Proof
Because $\operatorname{rot} \nabla p = 0$ in Ω and, according to Theorem 2.1, $\nabla p = \boldsymbol{f} - \sigma \boldsymbol{u} - \nu \operatorname{curl} \omega$ in Ω, it suffices to apply Lemma 4.11 to $\boldsymbol{\rho} = \nabla p$ and $\boldsymbol{\rho}_h = \mathbf{r}(\boldsymbol{u}_h, \omega_h)$ and then employ the triangle inequality. $\qquad \square$

The third term involving $\mathbf{r}(\boldsymbol{u}_h, \omega_h)$ is estimated next.

Lemma 4.13
There exists $C > 0$, independent of h, such that

$$h_e \, \| \mathbf{r}(\boldsymbol{u}_h, \omega_h) \cdot \boldsymbol{t} \|_{0,e}^2 \;\leqslant\; C \, \{ \|\boldsymbol{u} - \boldsymbol{u}_h\|_{0,T_e}^2 \,+\, |\omega - \omega_h|_{1,T_e}^2 \} \qquad \forall \, e \in \mathcal{E}_h(\Sigma) \,, \qquad (4.32)$$

where T_e is the triangle of $\mathcal{T}_h$ having e as an edge.

Proof
It follows as in the proof of [6, Lemma 21] (see also [41, Lemma 5.17]). In fact, given $e \in \mathcal{E}_h(\Sigma)$, we set $\gamma_e := \mathbf{r}(\boldsymbol{u}_h, \omega_h) \cdot \boldsymbol{t}$ on e. Because $p = 0$ on Σ (cf. Theorem 2.1), there holds $\nabla p \cdot \boldsymbol{t} = 0$ on Σ, and hence,

$$\mathbf{r}(\boldsymbol{u}_h, \omega_h) \cdot \boldsymbol{t} = \{ \mathbf{r}(\boldsymbol{u}_h, \omega_h) - \nabla p \} \cdot \boldsymbol{t} \quad \text{on} \quad e \,.$$

Then, applying (4.22) and the extension operator $L : C(e) \to C(T)$, we obtain that

$$\|\gamma_e\|_{0,e}^2 \;\leqslant\; c_2 \, \|\psi_e^{1/2} \, \gamma_e\|_{0,e}^2 = c_2 \int_e \psi_e \, \gamma_e \, \{ \mathbf{r}(\boldsymbol{u}_h, \omega_h) \cdot \boldsymbol{t} \}$$
$$= c_2 \int_{\partial T_e} \psi_e \, L(\gamma_e) \, \{ \{ \mathbf{r}(\boldsymbol{u}_h, \omega_h) - \nabla p \} \cdot \boldsymbol{t} \} \,. \qquad (4.33)$$

Now, integrating by parts and using that $\operatorname{rot} \{\nabla p\} = 0$ in Ω, we find that

$$\int_{\partial T_e} \psi_e \, L(\gamma_e) \, \{ \{ \mathbf{r}(\boldsymbol{u}_h, \omega_h) - \nabla p \} \cdot \boldsymbol{t} \}$$
$$= - \int_{T_e} \operatorname{curl}(\psi_e \, L(\gamma_e)) \cdot \{ \mathbf{r}(\boldsymbol{u}_h, \omega_h) - \nabla p \} + \int_{T_e} \psi_e \, L(\gamma_e) \, \operatorname{rot} \{ \mathbf{r}(\boldsymbol{u}_h, \omega_h) \} \,. \qquad (4.34)$$

In turn, thanks to the fact that $0 \leqslant \psi_e \leqslant 1$ and (4.23), we have that

$$\|\psi_e \, L(\gamma_e)\|_{0,T_e} \;\leqslant\; \|\psi_e^{1/2} \, L(\gamma_e)\|_{0,T_e} \;\leqslant\; c \, h_e^{1/2} \|\gamma_e\|_{0,e} \,. \qquad (4.35)$$

Hence, applying the Cauchy–Schwarz inequality and the inverse estimate (4.24) and recalling from Theorem 2.1 that $\nabla p = \boldsymbol{f} - \sigma \boldsymbol{u} - \nu \operatorname{curl} \omega$ in Ω, we deduce from (4.33)–(4.35) that

$$\|\gamma_e\|_{0,e}^2 \;\leqslant\; C \, \{ h_{T_e}^{-1} \, \{ \|\boldsymbol{u} - \boldsymbol{u}_h\|_{0,T_e} + |\omega - \omega_h|_{1,T_e} \} \,+\, \| \operatorname{rot} \{ \mathbf{r}(\boldsymbol{u}_h, \omega_h) \} \|_{0,T_e} \} \, h_e^{1/2} \|\gamma_e\|_{0,e} \,,$$

which, using that $h_e \leqslant h_{T_e}$, yields

$$h_e \, \|\gamma_e\|_{0,e}^2 \;\leqslant\; C \, \{ \|\boldsymbol{u} - \boldsymbol{u}_h\|_{0,T_e}^2 \,+\, |\omega - \omega_h|_{1,T_e}^2 \,+\, h_{T_e}^2 \, \| \operatorname{rot} \{ \mathbf{r}(\boldsymbol{u}_h, \omega_h) \} \|_{0,T_e}^2 \} \,.$$

This inequality and the upper bound for $h_{T_e}^2 \, \| \operatorname{rot} \{ \mathbf{r}(\boldsymbol{u}_h, \omega_h) \} \|_{0,T_e}^2$ (cf. (4.30)) imply (4.32) and complete the proof. $\qquad \square$

We continue our efficiency analysis with the estimates involving $\boldsymbol{u}_h \cdot \boldsymbol{t}$, which are provided in the following two lemmata.

Lemma 4.14
There exists $C > 0$, independent of h, such that

$$h_e \, \|[\boldsymbol{u}_h \cdot \boldsymbol{t}]\|_{0,e}^2 \, \leqslant \, C \sum_{T \subseteq w_e} \left\{ \|\boldsymbol{u} - \boldsymbol{u}_h\|_{0,T}^2 \, + \, h_T^2 \, \|\omega - \omega_h\|_{0,T}^2 \right\} \qquad \forall \, e \in \mathcal{E}_h(\Omega) \, . \qquad (4.36)$$

Proof
Given $e \in \mathcal{E}_h(\Omega)$, we set $\gamma_e := [\boldsymbol{u}_h \cdot \boldsymbol{t}]$ on e. Hence, applying (4.22) and then employing the extension operator $L : C(e) \to C(T)$ together with the integration by parts formula on each $T \subseteq w_e$, we obtain that

$$\|\gamma_e\|_{0,e}^2 \, \leqslant \, c_2 \, \|\psi_e^{1/2} \, \gamma_e\|_{0,e}^2 \, = \, c_2 \int_e \psi_e \, L(\gamma_e) \, [\boldsymbol{u}_h \cdot \boldsymbol{t}]$$
$$= \, c_2 \left\{ \int_{w_e} \operatorname{rot} \boldsymbol{u}_h \, \psi_e \, L(\gamma_e) - \int_{w_e} \boldsymbol{u}_h \cdot \operatorname{curl} \left\{ \psi_e \, L(\gamma_e) \right\} \right\} \, , \qquad (4.37)$$

where, after adding and subtracting both ω_h and ω, we can write

$$\int_{w_e} \operatorname{rot} \boldsymbol{u}_h \, \psi_e \, L(\gamma_e) \, = \, \int_{w_e} \left\{ \operatorname{rot} \boldsymbol{u}_h - \omega_h \right\} \psi_e \, L(\gamma_e) + \int_{w_e} (\omega_h - \omega) \, \psi_e \, L(\gamma_e) + \int_{w_e} \omega \, \psi_e \, L(\gamma_e) \, . \qquad (4.38)$$

In turn, recalling from Theorem 2.1 that $\omega = \operatorname{rot} \boldsymbol{u}$ in Ω, which ensures that $\boldsymbol{u} \cdot \boldsymbol{t}$ is continuous across the edges of $\mathcal{E}_h(\Omega)$, we can integrate by parts in w_e so that, using that ψ_e vanishes on ∂w_e, we find that

$$\int_{w_e} \omega \, \psi_e \, L(\gamma_e) \, = \, \int_{w_e} \operatorname{rot} \boldsymbol{u} \, \psi_e \, L(\gamma_e) \, = \, \int_{w_e} \boldsymbol{u} \cdot \operatorname{curl} \left\{ \psi_e \, L(\gamma_e) \right\} \, .$$

In this way, replacing the foregoing equality into (4.38) and then the resulting expression into (4.37), we arrive at

$$\|\gamma_e\|_{0,e}^2 \leqslant c_2 \left\{ \int_{w_e} \left\{ \operatorname{rot} \boldsymbol{u}_h - \omega_h \right\} \psi_e \, L(\gamma_e) + \int_{w_e} (\omega_h - \omega) \, \psi_e \, L(\gamma_e) \right.$$
$$\left. + \int_{w_e} (\boldsymbol{u} - \boldsymbol{u}_h) \cdot \operatorname{curl} \left\{ \psi_e \, L(\gamma_e) \right\} \right\} \, . \qquad (4.39)$$

Next, applying the Cauchy–Schwarz inequality, the inverse estimate (4.24), (4.23), and the fact that $h_e \leqslant h_T$ for each $T \subseteq w_e$, we deduce from (4.39) that

$$\|\gamma_e\|_{0,e}^2 \leqslant C \sum_{T \subseteq w_e} \left\{ \|\operatorname{rot} \boldsymbol{u}_h - \omega_h\|_{0,T} + \|\omega - \omega_h\|_{0,T} + h_T^{-1} \|\boldsymbol{u} - \boldsymbol{u}_h\|_{0,T} \right\} \|\psi_e \, L(\gamma_e)\|_{0,T}$$

$$\leqslant C \sum_{T \subseteq w_e} \left\{ h_e^{1/2} \|\operatorname{rot} \boldsymbol{u}_h - \omega_h\|_{0,T} + h_e^{1/2} \|\omega - \omega_h\|_{0,T} + h_T^{-1/2} \|\boldsymbol{u} - \boldsymbol{u}_h\|_{0,T} \right\} \|\gamma_e\|_{0,e} \, ,$$

which yields, after some simplifications,

$$h_e \, \|\gamma_e\|_{0,e}^2 \, \leqslant \, C \sum_{T \subseteq w_e} \left\{ h_T^2 \, \|\operatorname{rot} \boldsymbol{u}_h - \omega_h\|_{0,T}^2 + h_T^2 \, \|\omega - \omega_h\|_{0,T}^2 + \|\boldsymbol{u} - \boldsymbol{u}_h\|_{0,T}^2 \right\} \, .$$

This inequality and the efficiency estimate for $h_T^2 \, \|\operatorname{rot} \boldsymbol{u}_h - \omega_h\|_{0,T}^2$ (cf. Lemma 4.10) imply (4.36) and complete the proof. $\qquad \square$

Lemma 4.15
There exists $C > 0$, independent of h, such that

$$h_e \|\boldsymbol{a} \cdot \boldsymbol{t} - \boldsymbol{u}_h \cdot \boldsymbol{t}\|_{0,e}^2 \leqslant C \left\{ \|\boldsymbol{u} - \boldsymbol{u}_h\|_{0,T_e}^2 + h_{T_e}^2 \|\omega - \omega_h\|_{0,T_e}^2 \right\} \qquad \forall e \in \mathcal{E}_h(\Sigma), \quad (4.40)$$

where T_e is the triangle of $\mathcal{T}_h$ having e as an edge.

Proof
Given $e \in \mathcal{E}_h(\Sigma)$, we let T_e be the triangle of $\mathcal{T}_h$ having e as an edge and set $\gamma_e := \boldsymbol{a} \cdot \boldsymbol{t} - \boldsymbol{u}_h \cdot \boldsymbol{t}$ on e. Then, applying (4.22), employing the extension operator $L : C(e) \rightarrow C(T_e)$, and using that $\boldsymbol{u} \cdot \boldsymbol{t} = \boldsymbol{a} \cdot \boldsymbol{t}$ on Σ, we obtain

$$\|\gamma_e\|_{0,e}^2 \leqslant c_2 \|\psi_e^{1/2} \gamma_e\|_{0,e}^2 = c_2 \int_e \psi_e \gamma_e (\boldsymbol{a} \cdot \boldsymbol{t} - \boldsymbol{u}_h \cdot \boldsymbol{t}) = c_2 \int_{\partial T_e} \psi_e L(\gamma_e) (\boldsymbol{u} \cdot \boldsymbol{t} - \boldsymbol{u}_h \cdot \boldsymbol{t}). \quad (4.41)$$

Next, integrating by parts, employing from Theorem 2.1 that $\omega = \mathrm{rot}\,\boldsymbol{u}$, and adding and subtracting ω_h, we find that

$$\int_{\partial T_e} \psi_e L(\gamma_e)(\boldsymbol{u} \cdot \boldsymbol{t} - \boldsymbol{u}_h \cdot \boldsymbol{t}) = -\int_{T_e} \mathrm{curl}\,\{\psi_e L(\gamma_e)\}\,(\boldsymbol{u} - \boldsymbol{u}_h) + \int_{T_e} \psi_e L(\gamma_e)\,\{\mathrm{rot}\,\boldsymbol{u} - \mathrm{rot}\,\boldsymbol{u}_h\}$$

$$= -\int_{T_e} \mathrm{curl}\,\{\psi_e L(\gamma_e)\}\,(\boldsymbol{u} - \boldsymbol{u}_h) + \int_{T_e} \psi_e L(\gamma_e)\,\{\omega - \omega_h\} - \int_{T_e} \psi_e L(\gamma_e)\,\{\mathrm{rot}\,\boldsymbol{u}_h - \omega_h\}\,.$$

Thus, replacing the foregoing identity back into (4.41) and employing the Cauchy–Schwarz inequality, the inverse estimate (4.24), and (4.23), we deduce that

$$\|\gamma_e\|_{0,e}^2 \leqslant C \left\{ h_{T_e}^{-1} \|\boldsymbol{u} - \boldsymbol{u}_h\|_{0,T_e} + \|\omega - \omega_h\|_{0,T_e} + \|\mathrm{rot}\,\boldsymbol{u}_h - \omega_h\|_{0,T_e} \right\} h_e^{1/2} \|\gamma_e\|_{0,e}\,,$$

which, after minor manipulations, gives

$$h_e \|\gamma_e\|_{0,e}^2 \leqslant C \left\{ \|\boldsymbol{u} - \boldsymbol{u}_h\|_{0,T_e}^2 + h_{T_e}^2 \|\omega - \omega_h\|_{0,T_e}^2 + h_{T_e}^2 \|\mathrm{rot}\,\boldsymbol{u}_h - \omega_h\|_{0,T_e}^2 \right\}\,. \quad (4.42)$$

Finally, it is easy to see that (4.42) and the efficiency estimate for $h_T^2 \|\mathrm{rot}\,\boldsymbol{u}_h - \omega_h\|_{0,T}^2$ (cf. Lemma 4.10) imply (4.40), which ends the proof. $\qquad \square$

Consequently, the efficiency of θ follows straightforwardly from the estimates (4.19) and (4.20) and Lemmata 4.10 and 4.12–4.15. Similarly, in order to complete the efficiency estimate for $\boldsymbol{\vartheta}$, we just need to provide the corresponding upper bounds for the three remaining terms in (4.2). To this end, we now state the following preliminary result, which is the analogue of Lemma 4.11 when involving div and normal jump instead of rot and tangential jump, respectively.

Lemma 4.16
Let $\boldsymbol{\rho}_h \in \mathbf{L}^2(\Omega)$ be a piecewise polynomial of degree $k \geqslant 0$ on each $T \in \mathcal{T}_h$, and let $\boldsymbol{\rho} \in \mathbf{L}^2(\Omega)$ be such that div $\{\boldsymbol{\rho}\} = 0$ in Ω. Then, there exist c and $\widetilde{c} > 0$, independent of h, such that

$$h_T^2 \|\mathrm{div}\,\{\boldsymbol{\rho}_h\}\|_{0,T}^2 \leqslant c \|\boldsymbol{\rho} - \boldsymbol{\rho}_h\|_{0,T}^2 \qquad \forall T \in \mathcal{T}_h\,, \quad (4.43)$$

and

$$h_e \|[\boldsymbol{\rho}_h \cdot \boldsymbol{n}]\|_{0,e}^2 \leqslant \widetilde{c} \|\boldsymbol{\rho} - \boldsymbol{\rho}_h\|_{0,w_e}^2 \qquad \forall e \in \mathcal{E}_h(\Omega)\,. \quad (4.44)$$

Proof
It follows from slight modifications of the proofs of [40, Lemmata 4.5 and 4.6]. We omit further details. $\qquad \square$

The foregoing lemma allows us to establish the following efficiency estimates for $\boldsymbol{\vartheta}$.

Lemma 4.17
There exist C_1 and $C_2 > 0$, independent of h, such that

$$h_T^2 \|\operatorname{div}\{\mathbf{r}(\boldsymbol{u}_h, p_h)\}\|_{0,T}^2 \leqslant C_1 \{\|\boldsymbol{u} - \boldsymbol{u}_h\|_{0,T}^2 + |p - p_h|_{1,T}^2\} \qquad \forall \, T \in \mathcal{T}_h, \qquad (4.45)$$

and

$$h_e \|[\mathbf{r}(\boldsymbol{u}_h, p_h) \cdot \boldsymbol{n}]\|_{0,e}^2 \leqslant C_2 \{\|\boldsymbol{u} - \boldsymbol{u}_h\|_{0,w_e}^2 + |p - p_h|_{1,w_e}^2\} \qquad \forall \, e \in \mathcal{E}_h(\Omega). \qquad (4.46)$$

Proof
Because $\operatorname{div}\operatorname{curl}\omega = 0$ in Ω and, according to Theorem 2.1, $\nu \operatorname{curl}\omega = \boldsymbol{f} - \sigma\boldsymbol{u} - \nabla p$ in Ω, it suffices to apply Lemma 4.16 to $\boldsymbol{\rho} = \nu \operatorname{curl}\omega$ and $\boldsymbol{\rho}_h = \mathbf{r}(\boldsymbol{u}_h, p_h)$ and then employ the triangle inequality. $\qquad\square$

We conclude our efficiency analysis for $\boldsymbol{\vartheta}$ with the following result.

Lemma 4.18
There exists $C > 0$, independent of h, such that

$$h_e \|\mathbf{r}(\boldsymbol{u}_h, p_h) \cdot \boldsymbol{n}\|_{0,e}^2 \leqslant C \{\|\boldsymbol{u} - \boldsymbol{u}_h\|_{0,T_e}^2 + |p - p_h|_{1,T_e}^2\} \qquad \forall \, e \in \mathcal{E}_h(\Gamma), \qquad (4.47)$$

where T_e is the triangle of $\mathcal{T}_h$ having e as an edge.

Proof
It follows analogously to the proof of Lemma 4.13. In fact, given $e \in \mathcal{E}_h(\Gamma)$, we let T_e be the triangle of $\mathcal{T}_h$ having e as an edge and set $\gamma_e := \mathbf{r}(\boldsymbol{u}_h, p_h) \cdot \boldsymbol{n}$ on e. Because $\omega = 0$ on Γ (cf. Theorem 2.1), there holds $\operatorname{curl}\omega \cdot \boldsymbol{n} = \nabla\omega \cdot \boldsymbol{t} = 0$ on Γ, and hence,

$$\mathbf{r}(\boldsymbol{u}_h, p_h) \cdot \boldsymbol{n} = \{\mathbf{r}(\boldsymbol{u}_h, p_h) - \nu \operatorname{curl}\omega\} \cdot \boldsymbol{n} \quad \text{on} \quad e.$$

Then, applying (4.22) and the extension operator $L : C(e) \to C(T_e)$, we obtain that

$$\|\gamma_e\|_{0,e}^2 \leqslant c_2 \|\psi_e^{1/2} \gamma_e\|_{0,e}^2 = c_2 \int_e \psi_e \gamma_e \{\mathbf{r}(\boldsymbol{u}_h, p_h) \cdot \boldsymbol{n}\}$$
$$= c_2 \int_{\partial T_e} \psi_e L(\gamma_e) \{\{\mathbf{r}(\boldsymbol{u}_h, p_h) - \nu \operatorname{curl}\omega\} \cdot \boldsymbol{n}\}. \qquad (4.48)$$

Now, integrating by parts and using that $\operatorname{div}\{\operatorname{curl}\omega\} = 0$ in Ω, we find that

$$\int_{\partial T_e} \psi_e L(\gamma_e) \{\{\mathbf{r}(\boldsymbol{u}_h, p_h) - \nu \operatorname{curl}\omega\} \cdot \boldsymbol{n}\}$$
$$= \int_{T_e} \nabla(\psi_e L(\gamma_e)) \cdot \{\mathbf{r}(\boldsymbol{u}_h, p_h) - \nu \operatorname{curl}\omega\} + \int_{T_e} \psi_e L(\gamma_e) \operatorname{div}\{\mathbf{r}(\boldsymbol{u}_h, p_h)\}. \qquad (4.49)$$

On the other hand, using that $0 \leqslant \psi_e \leqslant 1$ and (4.23), we have that

$$\|\psi_e L(\gamma_e)\|_{0,T_e} \leqslant \|\psi_e^{1/2} L(\gamma_e)\|_{0,T_e} \leqslant c \, h_e^{1/2} \|\gamma_e\|_{0,e}. \qquad (4.50)$$

Hence, applying the Cauchy–Schwarz inequality and the inverse estimate (4.24) and recalling from Theorem 2.1 that $\nu \operatorname{curl}\omega = \boldsymbol{f} - \sigma\boldsymbol{u} - \nabla p$ in Ω, we deduce from (4.48)–(4.50) that

$$\|\gamma_e\|_{0,e}^2 \leqslant C \{h_{T_e}^{-1} \{\|\boldsymbol{u} - \boldsymbol{u}_h\|_{0,T_e} + |p - p_h|_{1,T_e}\} + \|\operatorname{div}\{\mathbf{r}(\boldsymbol{u}_h, p_h)\}\|_{0,T_e}\} h_e^{1/2} \|\gamma_e\|_{0,e},$$

which yields

$$h_e \|\gamma_e\|_{0,e}^2 \leqslant C \{\|\boldsymbol{u} - \boldsymbol{u}_h\|_{0,T_e}^2 + |p - p_h|_{1,T_e}^2 + h_{T_e}^2 \|\operatorname{div}\{\mathbf{r}(\boldsymbol{u}_h, p_h)\}\|_{0,T_e}^2\},$$

where we have also employed that $h_e \leqslant h_{T_e}$. The foregoing inequality and the upper bound for $h_{T_e}^2 \|\operatorname{div}\{\mathbf{r}(\boldsymbol{u}_h, p_h)\}\|_{0,T_e}^2$ (cf. Lemma 4.17) imply (4.47) and complete the proof. $\qquad\square$

We end this section by remarking that the efficiency of $\boldsymbol{\vartheta}$ follows from the corresponding esti-mate of $\boldsymbol{\theta}$ together with Lemmata 4.17 and 4.18. Alternatively, we could have first provided all the estimates yielding the efficiency of $\boldsymbol{\vartheta}$ and then conclude the one of $\boldsymbol{\theta}$ from the fact that $\boldsymbol{\theta} \leqslant \boldsymbol{\vartheta}$.

5. NUMERICAL EXPERIMENTS

We now turn to the presentation of selected numerical examples confirming our theoretical findings. The solutions of the involved unsymmetric linear systems are computed with the multifrontal mas-sively parallel sparse direct solver MUMPS. Given the solution $(\boldsymbol{u}, \omega, p) \in \mathbf{H}_\Gamma(\mathrm{div}; \Omega) \times \mathrm{H}_\Gamma^1(\Omega) \times \mathrm{H}_\Sigma^1(\Omega)$ of our continuous augmented formulation (2.3), we measure the accuracy of the numerical scheme by the errors

$$e(\boldsymbol{u}) := \|\boldsymbol{u} - \boldsymbol{u}_h\|_{\mathrm{div},\Omega}, \; e(\omega) := \|\omega - \omega_h\|_{1,\Omega}, \; e(p) := \|p - p_h\|_{1,\Omega},$$

where $(\boldsymbol{u}_h, \omega_h, p_h) \in \mathbb{H}_h$ is the solution of the augmented Galerkin scheme (3.2). In turn, the associated observed convergence rates are computed as $r(\cdot) := \frac{\log(e(\cdot)/\hat{e}(\cdot))}{\log(h/\hat{h})}$, where e and $\hat{e}$ denote the errors associated with two consecutive meshes of sizes h and $\hat{h}$. To this respect, in what follows, N denotes the number of degrees of freedom associated with a given triangulation. Bear in mind that the aforementioned notations are also employed later on in Section 5.2 for the case of a reference solution $(\boldsymbol{u}_{\mathrm{ref}}, \omega_{\mathrm{ref}}, p_{\mathrm{ref}})$ instead of $(\boldsymbol{u}, \omega, p)$. Furthermore, concerning the stabilization coefficients,
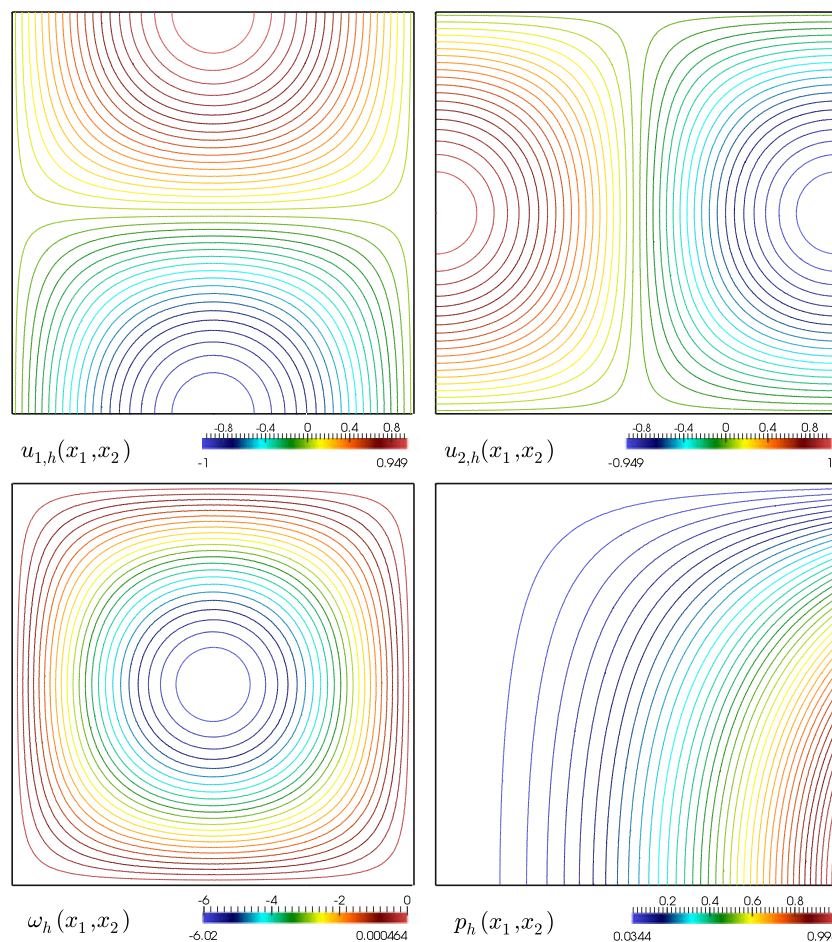

Figure 1. Example 1: Contour plots of the approximated velocity components (top), vorticity (bottom left), and pressure (bottom right), computed with an augmented $\mathbf{RT}_0 - P_1 - P_1$ family for the Brinkman problem on a structured mesh of 155 652 elements and 77 827 vertices.

in Examples 1–3 as follows, we consider the optimal values described at the end of Section 3, that is, $\kappa_1 = \frac{\nu}{2\sigma}$, $\kappa_2 = \frac{1}{2\sigma}$, and $\kappa_3 = \frac{\sigma}{2}$, where σ and ν are the model parameters.

5.1. Example 1: convergence tests against analytical solutions

We consider $\Omega = (0, 1)^2$, and the boundary is split into Γ (bottom and right lids of the square) and Σ (top and left sides of the square). A sequence of uniformly refined meshes is used to compute these errors and rates with respect to the following exact solutions of (1.1):

$$\boldsymbol{u} = \begin{pmatrix} -\sin(\pi x_1)\cos(\pi x_2) \\ \sin(\pi x_2)\cos(\pi x_1) \end{pmatrix}, \quad \omega = -2\pi \sin(\pi x_2)\sin(\pi x_1), \quad p = x_1^2(1 - x_2^2),$$

satisfying the set of boundary data

$$\begin{cases} \omega = 0, \ \boldsymbol{u} \cdot \boldsymbol{n} = 0 & \text{on } \Gamma, \\ p = 0, \ \boldsymbol{u} \cdot \boldsymbol{t} = \sin(\pi x_1)\cos(\pi x_2)n_2 + \sin(\pi x_2)\cos(\pi x_1)n_1 & \text{on } \Sigma. \end{cases}$$

Model parameters assume the values $\sigma = 0.1$ and $\nu = 0.01$. The error history and the effectivity indexes for $\boldsymbol{\theta}$ and $\boldsymbol{\vartheta}$ are presented in Table I for two finite element families using $\mathbf{RT}_0 - P_1 - P_1$ ($k = 0$) and $\mathbf{RT}_1 - P_2 - P_2$ ($k = 1$) approximations for velocity, vorticity, and pressure. The table shows that the accuracy of the schemes approaches asymptotically an order $O(h^{k+1})$ for the

Table I. Example 1: convergence tests against analytical solutions employing $\mathbf{RT}_0 - P_1 - P_1$ (top rows) and $\mathbf{RT}_1 - P_2 - P_2$ (bottom rows) finite element approximations of velocity–vorticity–pressure formulation, computed on a sequence of uniformly refined triangulations of the unit square.

| N	h	$e(\omega)$	$r(\omega)$	$e(\boldsymbol{u})$	$r(\boldsymbol{u})$	$e(p)$	$r(p)$	$\texttt{eff}(\boldsymbol{\theta})$	$\texttt{eff}(\boldsymbol{\vartheta})$
				$\mathbf{RT}_0 - P_1 - P_1$ finite elements					
34	0.707107	8.663562	—	1.128531	—	0.566262	—	3.394480	2.348912
289	0.202031	3.042580	0.835291	0.165443	1.532650	0.134389	1.148111	2.916250	2.372894
1378	0.088388	1.361391	0.972808	0.069581	1.047711	0.057595	1.024953	2.773871	2.302962
4381	0.048766	0.754373	0.992713	0.038304	1.003762	0.031624	1.008094	2.741535	2.284435
10 858	0.030743	0.476180	0.997276	0.024144	1.000363	0.019908	1.003083	2.730383	2.277252
22 849	0.021107	0.327081	0.998753	0.016576	0.999982	0.013661	1.001377	2.725384	2.273743
42 874	0.015371	0.238253	0.999348	0.012072	0.999939	0.009947	1.000691	2.722743	2.271742
73 933	0.011687	0.181164	0.999625	0.009179	0.999947	0.007562	1.000380	2.721174	2.270497
119 506	0.009183	0.142352	0.999768	0.007212	0.999959	0.005941	1.000236	2.720171	2.269654
183 553	0.007404	0.114783	0.999849	0.005815	0.999969	0.004790	1.000146	2.719482	2.269063
270 514	0.006095	0.094499	0.999897	0.004787	0.999977	0.003943	1.000109	2.718991	2.268634
385 309	0.005105	0.079148	0.999928	0.004009	0.999982	0.003302	1.000070	2.719032	2.268943
533 338	0.004338	0.067252	0.999947	0.003407	0.999986	0.002806	1.000051	2.719193	2.269012
720 481	0.003731	0.057847	0.999966	0.002361	0.999991	0.002412	1.000030	2.719145	2.269160
				$\mathbf{RT}_1 - P_2 - P_2$ finite elements					
98	0.707107	2.753852	—	0.217709	—	0.097066	—	0.180569	0.167872
968	0.202031	0.266276	1.864870	0.014382	2.168913	0.006625	2.142810	0.496039	0.394618
4802	0.088388	0.052312	1.968457	0.002687	2.029184	0.001268	1.999322	0.496915	0.394605
15 488	0.048766	0.016037	1.988121	$8.8152e-4$	2.004256	$3.8728e-4$	1.993636	0.503835	0.406301
38 642	0.030743	0.006391	1.993864	$3.2410e-4$	1.999490	$1.5439e-4$	1.995983	0.497461	0.397375
81 608	0.021107	0.003017	1.996242	$1.5298e-4$	1.998673	$7.2847e-5$	1.997344	0.491595	0.391526
153 458	0.015371	0.001601	1.997451	$8.1170e-5$	1.998665	$3.8658e-5$	1.998127	0.501924	0.411273
264 992	0.011687	$9.2632e-4$	1.998167	$4.6939e-5$	1.998834	$2.2357e-5$	1.998628	0.484082	0.384070
428 738	0.009183	$5.7205e-4$	1.998650	$2.8985e-5$	1.999021	$1.3805e-5$	1.998921	0.509795	0.406397
658 952	0.007404	$3.7197e-4$	1.998927	$1.8846e-5$	1.999152	$8.9766e-6$	1.999143	0.505238	0.405025
971 618	0.006095	$2.3062e-4$	1.999289	$9.1407e-6$	1.999378	$4.0412e-6$	1.999587	0.504564	0.404027
1 384 448	0.005105	$1.0793e-4$	1.999712	$4.8532e-6$	1.999629	$2.0237e-6$	1.999764	0.504027	0.403340
1 916 882	0.004338	$7.2521e-5$	1.999934	$2.4129e-6$	1.999917	$1.0168e-6$	1.999902	0.503735	0.404102
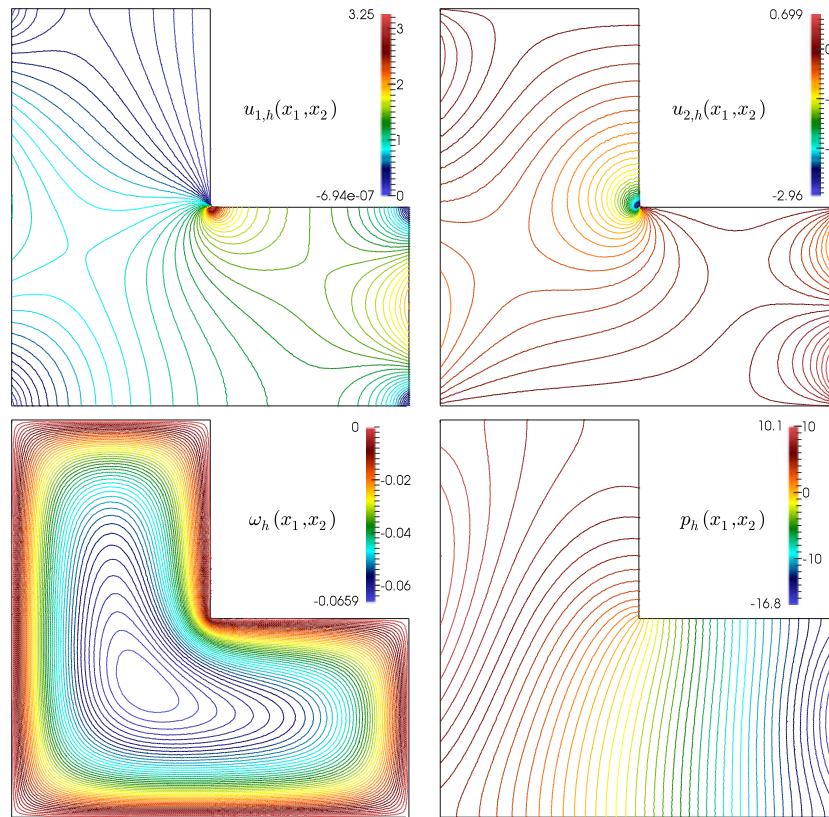
Figure 2. Example 2: Contour plots of the approximated velocity components, vorticity, and pressure, computed with an augmented **BDM**$_1 - P_1 - P_1$ family for the Brinkman problem.

vorticity and pressure in the H$^1(\Omega)$-norm and for the velocity in the **H**(div; Ω)-norm. In addition, the last two columns of Table I show that `eff`($\boldsymbol{\theta}$) and `eff`($\boldsymbol{\vartheta}$) remain always bounded, which confirms the reliability and efficiency of both a posteriori error estimators. Approximate solutions are portrayed in Figure 1.

5.2. *Example 2: experimental convergence with respect to a reference solution*

Our next test focuses on the mixed **BDM**$_1 - P_1 - P_1$ approximations of problem (1.1) defined on the nonconvex L-shaped domain $\Omega = (-1, 1)^2 \setminus (0, 1)^2$. The forcing term is $\boldsymbol{f} = (x_2, 0)^{\mathrm{t}}$, and the following boundary conditions are applied on $\Gamma = \partial\Omega$ (see, e.g., [10])

$$\omega = \omega_0 = 0 \text{ on } \Gamma \quad \text{and} \quad \boldsymbol{u} \cdot \boldsymbol{n} = \begin{cases} x_2^2 - 1 & \text{if } x_1 = -1, \ -1 \leqslant x_2 \leqslant 1, \\ -8x_2(1 + x_2) & \text{if } x_1 = 1, \ -1 \leqslant x_2 \leqslant 0, \\ 0 & \text{elsewhere on } \Gamma. \end{cases}$$

We set $\sigma = 10$ and $\nu = 0.1$, and notice that even for a smooth imposed normal velocity on the boundary, we expect the nonconvexity of the domain to yield high velocity gradients and degenerate convergence to the exact solution. This is verified in Figure 2 where approximate velocity components, vorticity, and pressure are displayed for a mesh of 57 898 elements and 28 950 vertices and from Table II, where experimental errors (computed with respect to a fine reference solution) are reported, exhibiting suboptimal convergence rates.

5.3. *Example 3: a posteriori error estimation and mesh adaptation*

Our third example illustrates the properties of the error estimators introduced and analyzed in Section 4. Again, the domain corresponds to the nonconvex L-shaped region $\Omega = (-1, 1)^2 \setminus (0, 1)^2$,

Table II. Example 2: experimental convergence test against a reference solution ($u_{\text{ref}}, \omega_{\text{ref}}, p_{\text{ref}}$), employing $\mathbf{BDM}_1 - P_1 - P_1$ finite element approximations of velocity–vorticity–pressure formulation.

N	h	$e(\omega_{\text{ref}})$	$r(\omega_{\text{ref}})$	$e(u_{\text{ref}})$	$r(u_{\text{ref}})$	$e(p_{\text{ref}})$	$r(p_{\text{ref}})$
42	1.414210	0.247112	—	2.335145	—	7.055480	—
130	0.750000	0.169301	0.596228	1.806842	0.814551	4.956274	0.556796
746	0.298142	0.078222	0.836976	1.475021	0.631235	2.595472	0.701229
2858	0.166875	0.038948	1.201621	0.928274	0.798003	1.578463	0.856964
8346	0.094886	0.023732	0.877510	0.560912	0.892308	1.120087	0.607639
18 698	0.067183	0.016746	1.009847	0.421598	0.827015	0.823019	0.892604
37 306	0.053650	0.012341	1.357252	0.261197	1.728470	0.596361	1.032152
68 186	0.036060	0.009533	0.649707	0.169668	1.086827	0.466019	0.620729
114 682	0.026678	0.008064	0.555524	0.103668	1.633632	0.377620	0.697997
187 418	0.022005	0.006808	0.879075	0.083456	1.348910	0.303283	1.138433
278 130	0.018275	0.004156	0.754791	0.064739	1.081331	0.265899	0.846078

on which the following exact solutions of (1.1) can be considered:

$$\mathbf{u} = \begin{pmatrix} -\sin(x_1)\cos(x_2) \\ \sin(x_2)\cos(x_1) \end{pmatrix}, \quad \omega = -2\sin(x_2)\sin(x_1), \quad p = \frac{1 - x_1}{(x_1 - x_a)^2 + (x_2 - x_b)^2},$$

with $x_a = x_b = 0.05$, and forcing terms are constructed according to these functions. Model parameters are chosen as $\sigma = 1$ and $\nu = 0.01$. The boundary Γ is the inner corner of the domain ($x_1 = 0$ and $x_2 = 0$) where we impose $w = 0$ and $\mathbf{u} \cdot \mathbf{n} = 0$, whereas Σ is formed by the remaining segments of $\partial\Omega$ where we set $p = 0$ and $\mathbf{u} \cdot \mathbf{t} = \sin(x_2)\cos(x_1)t_2 - \sin(x_1)\cos(x_2)t_1$. We analyze the accuracy of the finite element approximation first on a sequence of uniformly refined grids and secondly, on meshes adaptively refined according to the global a posteriori error estimators (4.3). Mesh refinement was implemented according to the well-known blue–green strategy (see details in, e.g., [25, 39, 41]). For this example, we compute the individual convergence rates as

$$r(\cdot) := -2\log(e(\cdot)/\hat{e}(\cdot))[\log(N/\hat{N})]^{-1},$$

where N and $\hat{N}$ denote the corresponding degrees of freedom at each triangulation, and we also define the total error, its convergence rate, and the effectivity index associated with a given global estimator $\zeta \in \{\theta, \vartheta\}$ as

$$\mathtt{e} := \left\{[e(\omega)]^2 + [e(\mathbf{u})]^2 + [e(p)]^2\right\}^{1/2}, \quad \mathtt{r} := -2\log(\mathtt{e}/\hat{\mathtt{e}})[\log(N/\hat{N})]^{-1}, \quad \mathtt{eff}(\zeta) := \mathtt{e}\,\zeta^{-1}.$$

These quantities are displayed in Table III, where we can observe that the total error converges suboptimally under quasi-uniform refinement, whereas convergence rates slightly above the optimal and stable effectivity indexes are attained for both cases of adaptive mesh refinement. Approximate solutions computed with an augmented $\mathbf{RT}_0 - P_1 - P_1$ family are depicted in Figure 3, and some adapted meshes are presented in Figure 4, showing a qualitative equivalence between the two different indicators in this particular example.

5.4. Example 4: flow in a contracting channel with a porous obstacle

We finally analyze the patterns of the flow within a channel with a sudden contraction and in the presence of a porous obstacle, as studied in, for example, [42]. For the boundary conditions, we put $\Gamma = \Gamma_{\text{wall}} \cup \Gamma_{\text{in}} \cup \Gamma_{\text{out}} = \partial\Omega$ and $\Sigma = \emptyset$ (see the sketch in Figure 5) and specify a normal Poiseuille velocity inflow and outflow on Γ_{in} and Γ_{out}, respectively, (along with compatible vorticity in each case) and impose slip conditions elsewhere. That is,

$$\mathbf{u} \cdot \mathbf{n} = \begin{cases} \alpha_{\text{in}}x_1(x_1 - 3/2) & \text{on } \Gamma_{\text{in}}, \\ \alpha_{\text{out}}x_1(x_1 - 3/5) & \text{on } \Gamma_{\text{out}}, \\ 0 & \text{on } \Gamma_{\text{wall}}, \end{cases} \qquad \omega = \omega_0 = \begin{cases} \alpha_{\text{in}}(2x_1 - 3/2) & \text{on } \Gamma_{\text{in}}, \\ \alpha_{\text{out}}(2x_1 - 3/5) & \text{on } \Gamma_{\text{out}}, \\ 0 & \text{on } \Gamma_{\text{wall}}, \end{cases}$$

Table III. Example 3: convergence tests against analytical solutions employing augmented $\mathbf{RT}_0 - P_1 - P_1$ finite element approximations of velocity–vorticity–pressure formulation, computed on a sequence of quasi-uniformly refined triangulations (top rows), adaptively refined according to the estimator $\boldsymbol{\theta}$ (middle rows), and adaptively refined according to $\boldsymbol{\vartheta}$ (bottom rows), defined as in (4.3).

N	$e(\omega)$	$r(\omega)$	$e(\boldsymbol{u})$	$r(\boldsymbol{u})$	$e(p)$	$r(p)$	e	r	eff($\boldsymbol{\theta}$)	eff($\boldsymbol{\vartheta}$)
					Quasi-uniform refinement					
89	92.10302	—	10.12382	—	289.6016	—	304.0633	—	1.049541	0.408742
709	252.2121	−0.96887	8.126014	0.211425	476.9278	−0.47983	539.5714	−0.55162	1.131525	0.416326
2601	42.98782	2.561512	4.570156	0.833185	428.0051	0.156683	430.1825	0.327997	1.005256	0.418037
7022	4.632165	4.476213	1.619454	2.084456	303.1442	0.693022	303.1837	0.702955	1.000183	0.418771
15617	1.218119	4.650495	1.025913	1.589383	238.2463	0.838741	238.2518	0.839119	1.000054	0.419946
30321	0.106278	5.804742	0.713606	0.863941	199.2018	0.425991	199.2025	0.426029	1.000029	0.414001
53534	0.047772	3.541487	0.466607	1.881665	161.2695	0.935575	161.2796	0.935585	1.000022	0.411894
88826	0.020123	3.345247	0.230782	2.724687	116.2435	1.266874	116.2435	0.866883	1.000015	0.416477
140517	0.014175	1.636090	0.173017	1.345333	99.00490	0.749465	99.00557	0.749462	1.000012	0.412909
206827	0.011403	1.612655	0.118302	2.816462	83.28521	1.286590	86.22232	0.856591	1.005052	0.419079
					Adaptive refinement using $\boldsymbol{\theta}$					
89	91.38271	—	10.27454	—	282.7271	—	285.6762	—	1.024215	—
188	71.50388	1.175420	9.124144	0.673578	250.2252	0.299417	270.4011	0.280289	1.041294	—
504	25.70819	4.443125	5.657072	0.987094	462.3110	−0.82570	463.0594	−0.81083	1.001823	—
1016	1.418674	8.264953	1.110110	4.645723	249.7937	1.756236	249.7999	1.760776	1.000051	—
2534	0.137455	5.108032	0.274131	3.060665	110.9823	1.775375	110.9811	1.775424	1.000010	—
9204	0.104376	0.426865	0.090156	1.724353	42.56176	1.486073	42.56193	1.486076	0.999961	—
43 700	0.069303	0.525783	0.039856	1.048030	16.33914	1.229231	16.33932	1.229225	0.999866	—
280 832	0.047708	0.401391	0.024232	0.534934	5.900880	1.094882	5.901128	1.094853	0.999493	—
828 623	0.028216	0.730731	0.016523	1.588990	2.477021	1.404517	1.565234	1.164862	1.000005	—
					Adaptive refinement using $\boldsymbol{\vartheta}$					
89	91.38270	—	16.27453	—	281.7279	—	283.6763	—	—	0.198789
188	84.36767	1.277472	12.40693	1.202951	269.7647	0.202557	269.9575	0.263561	—	0.417859
512	42.30257	1.668225	4.138492	1.963533	428.4066	-0.85802	432.5095	-0.87233	—	0.416173
1203	0.245006	12.06055	0.825899	3.773178	220.0954	1.559356	220.0964	1.357074	—	0.415403
3343	0.127734	1.274562	0.188241	2.893694	88.79212	1.776354	88.79233	1.776362	—	0.416205
11 663	0.101293	0.371224	0.078261	1.404779	33.09974	1.579423	33.15476	1.579393	—	0.414196
58 891	0.065322	0.541827	0.036403	0.945358	12.31275	1.221414	12.31292	1.221401	—	0.415953
411 923	0.047788	0.321364	0.024208	0.419442	4.463042	1.043427	4.463361	1.143036	—	0.414526
954 725	0.028276	0.712833	0.017525	0.662607	3.159851	1.070844	2.725254	1.261190	—	0.415151

with $\alpha_{in} = 2/75$ and $\alpha_{out} = 5/12$, ensuring that the flow rates at the inflow and outflow boundaries coincide, and we take $\nu = 1$.

We further assume that the coefficient σ (which is proportional to the inverse permeability of the medium) is possibly discontinuous

$$\sigma(x_1, x_2) = \begin{cases} \sigma_0 + \sigma_1 & \text{on the porous obstacle,} \\ \sigma_0 & \text{otherwise,} \end{cases}$$

where $\sigma_0 = 0.001$ and $\sigma_1 \in \{0.001, 0.1, 10, 1000\}$, and focus first on the case where the permeabilities inside and outside the obstacle differ by six orders of magnitude. There, we expect velocity patterns avoiding the obstacle and vanishing of the vorticity due to Darcy regime with constant permeability inside the obstacle. These phenomena can be indeed observed from Figure 6, where we plot contours of velocity components, vorticity, and pressure obtained with a $\mathbf{BDM}_1 - P_1 - P_1$ approximation. The unstructured mesh consists of 125 670 triangles and 62 696 nodes.

Next, using the same finite element family and the same mesh, we perform a qualitative comparison of the flow patterns depending on the value of the inverse permeability σ_1. The three panels in
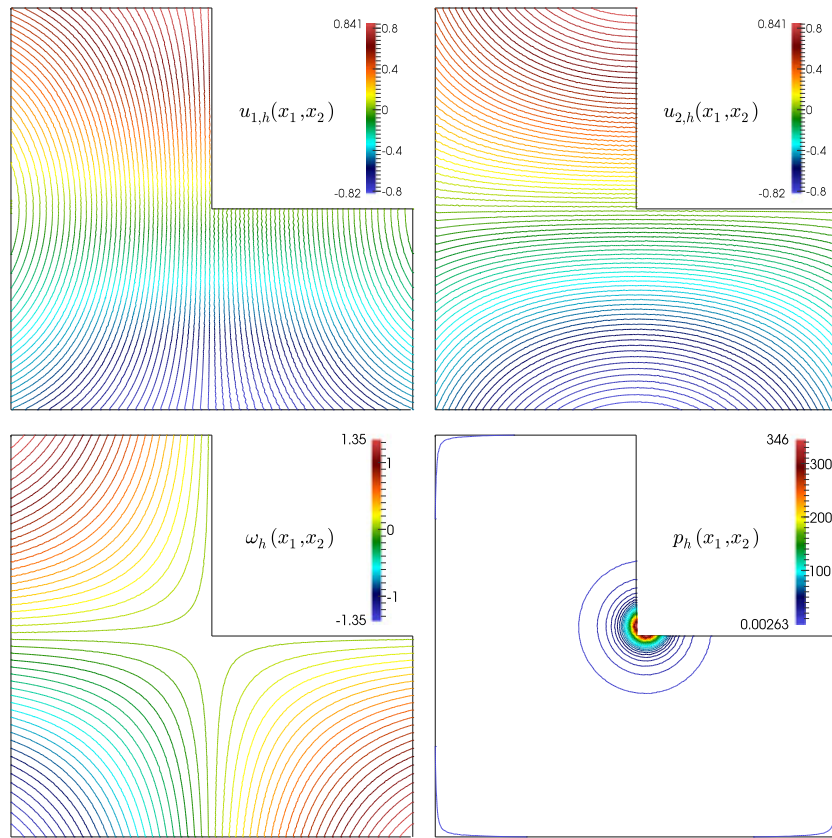
Figure 3. Example 3: contour plots of the approximate solutions computed with an augmented $\mathbf{RT}_0-P_1-P_1$ family for the Brinkman problem on an unstructured mesh.
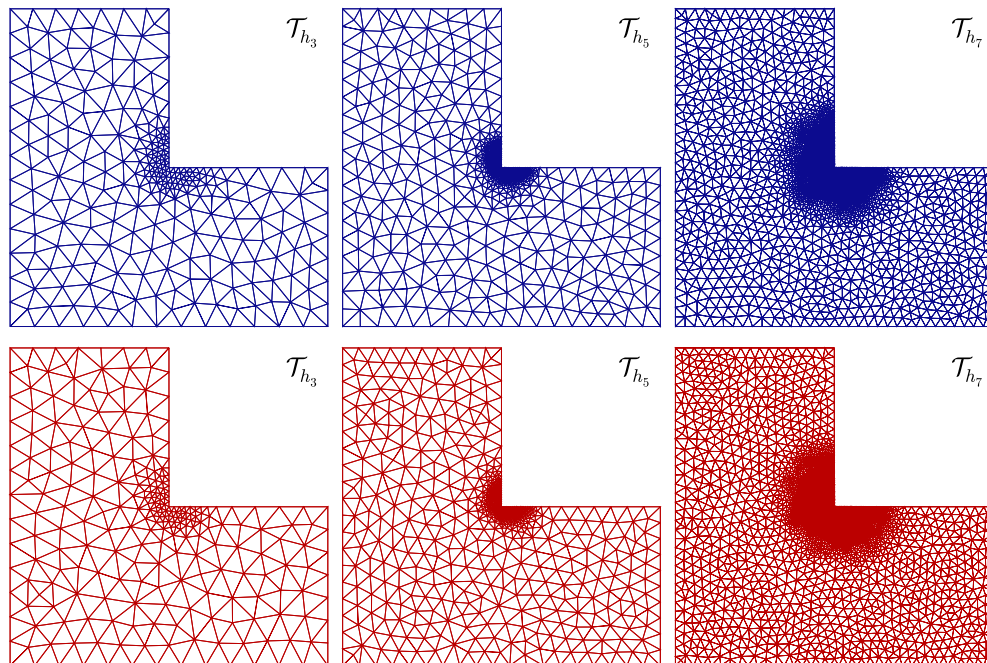

Figure 4. Example 3: successively refined meshes according to the indicators $\boldsymbol{\theta}$ and $\boldsymbol{\vartheta}$ (top and bottom panels, respectively).
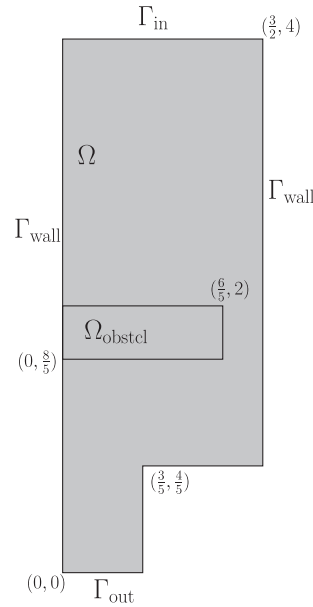
Figure 5. Example 4: Sketch of the domain and boundaries employed for the simulation of flow in a channel with sudden contraction.
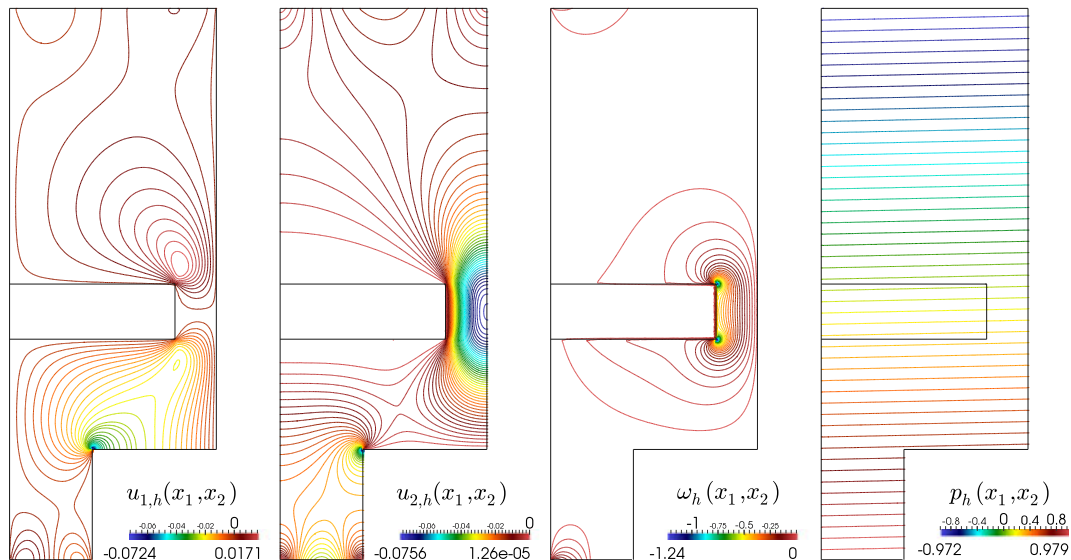

Figure 6. Example 4: contour plots of the approximated velocity components, vorticity, and pressure, computed with an augmented $\mathbf{BDM}_1 - P_1 - P_1$ family for the Brinkman problem.

Figure 7 indicates that if the difference between the permeability inside and outside the obstacle is small, the flow (velocity and vorticity) in the porous part is practically identical to that in the rest of the domain. However, as σ_1 increases, the zeroth-order term in the Brinkman problem is dominant, and the flow gradually avoids the porous obstacle. In all cases, the stabilization parameters were chosen as $\kappa_1 = 0.5\nu\sigma_0\sigma_1^{-2}$, $\kappa_2 = 0.5\sigma_0\sigma_1^{-2}$, and $\kappa_3 = 0.5\sigma_0$. Actually, even though our analysis for the continuous and discrete augmented formulations was carried out for a constant σ, it can be straightforwardly adapted to cover Example 4, where a discontinuous coefficient accompanying the zeroth-order velocity term is employed (interpreted here as the inverse permeability of the porous medium). In this case (and in the light of the proof of Lemma 2.2), it suffices to require $\sigma = \sigma(\boldsymbol{x}) \in \mathrm{L}^\infty(\Omega)$ with $0 < \sigma_{\min} \leqslant \sigma(\boldsymbol{x}) \leqslant \sigma_{\max}$ for $\boldsymbol{x} \in \mathbb{R}^2$, and so the stabilization parameters
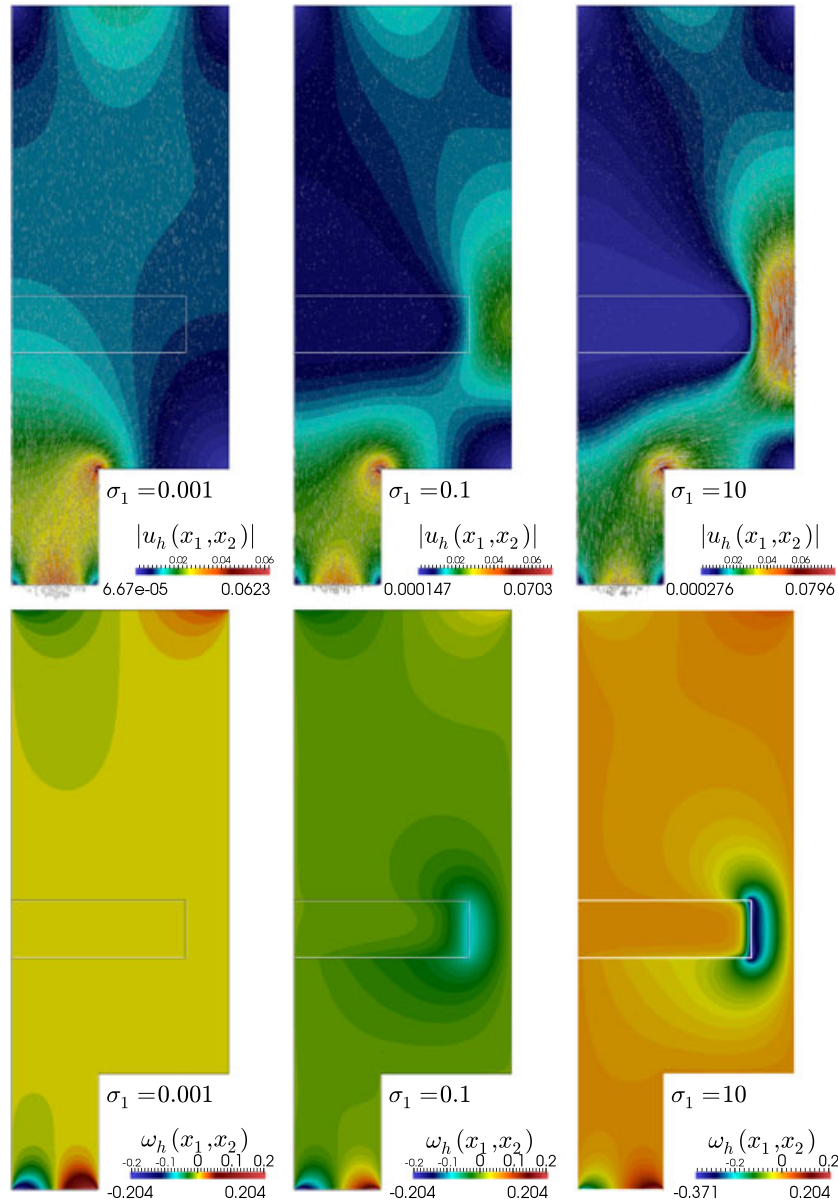
Figure 7. Example 4: velocity magnitude with vector representation (top panels) and vorticity field (bottom panels) for different values of the inverse permeability σ_1 on the porous obstacle. Solutions were computed with an augmented $\mathbf{BDM}_1 - P_1 - P_1$ family.

need to satisfy $0 < \kappa_1 < \frac{\nu\sigma_{\min}}{\sigma_{\max}^2}$, $0 < \kappa_2 < \frac{\sigma_{\min}}{\sigma_{\max}^2}$ and $\kappa_3 > 0$. However, similar to the discussion at the end of Section 3, the optimal values are given by the midpoints of the intervals for κ_1 and κ_2, and $\kappa_3 \geqslant 0.5\sigma_{\min}$.

REFERENCES

1. Burman E, Hansbo P. Edge stabilization for the generalized Stokes problem: a continuous interior penalty method. *Computer Methods in Applied Mechanics and Engineering* 2006; **195**(19–22):2393–2410.
2. Nafa K, Wathen AJ. Local projection stabilized Galerkin approximations for the generalized Stokes problem. *Computer Methods in Applied Mechanics and Engineering* 2009; **198**(5–8):877–883.
3. Bustinza R, Gatica GN, González M. A mixed finite element method for the generalized Stokes problem. *International Journal for Numerical Methods in Fluids* 2005; **49**(8):877–903.
4. Howell JS. Approximation of generalized Stokes problems using dual-mixed finite elements without enrichment. *International Journal for Numerical Methods in Fluids* 2011; **67**(2):247–268.
5. Barrios TP, Bustinza R, García G, Hernández E. On stabilized mixed methods for generalized Stokes problem based on the velocity-pseudostress formulation: a priori error estimates. *Computer Methods in Applied Mechanics and Engineering* 2012; **237/240**:78–87.
6. Gatica GN, Gatica LF, Márquez A. Analysis of a pseudostress-based mixed finite element method for the Brinkman model of porous media flow. *Numerische Mathematik* 2014; **126**(4):635–377.
7. Gatica GN, Márquez A, Sánchez MA. Analysis of a velocity-pressure-pseudostress formulation for the stationary Stokes equations. *Computer Methods in Applied Mechanics and Engineering* 2010; **199**(17–20):1064–1079.
8. Gatica GN, Márquez A, Sánchez MA. A priori and a posteriori error analyses of a velocity-pseudostress formulation for a class of quasi-Newtonian Stokes flows. *Computer Methods in Applied Mechanics and Engineering* 2011; **200**(17–20):1619–1636.
9. Amara M, Chacón Vera E, Trujillo D. Vorticity–velocity–pressure formulation for Stokes problem. *Mathematics of Computation* 2004; **73**(248):1673–1697.
10. Amoura K, Bernardi C, Chorfi N. Spectral element discretization of the vorticity, velocity and pressure formulation of the Stokes problem. *ESAIM: Mathematical Modelling and Numerical Analysis* 2006; **40**(5):897–921.
11. Bernardi C, Chorfi N. Spectral discretization of the vorticity, velocity, and pressure formulation of the Stokes problem. *SIAM Journal on Numerical Analysis* 2007; **44**(2):826–850.
12. Bochev PV, Gunzburger M. *Least-squares Finite Element Methods*, Applied Mathematical Sciences, vol. 166. Springer Verlag, 2009.
13. Chang CL, Jiang B-N. An error analysis of least-squares finite element method of velocity-pressure-vorticity formulation for the Stokes problem. *Computer Methods in Applied Mechanics and Engineering* 1990; **84**(3): 247–255.
14. Cockburn B, Cui J. An analysis of HDG methods for the vorticity-velocity-pressure formulation of the Stokes problem in three dimensions. *Mathematics of Computation* 2012; **81**(279):1355–1368.
15. Duan H-Y, Liang G-P. On the velocity-pressure-vorticity least-squares mixed finite element method for the 3D Stokes equations. *SIAM Journal on Numerical Analysis* 2003; **41**(6):2114–2130.
16. Dubois F, Salaün M, Salmon S. First vorticity-velocity-pressure numerical scheme for the Stokes problem. *Computer Methods in Applied Mechanics and Engineering* 2003; **192**(44–46):4877–4907.
17. Pontaza JP, Reddy JN. Spectral/hp least-squares finite element formulation for the Navier-Stokes equations. *Journal of Computational Physics* 2003; **190**(2):523–549.
18. Salaün M, Salmon S. Low-order finite element method for the well-posed bidimensional Stokes problem. *IMA Journal on Numerical Analysis* 2015; **35**(1):427–453.
19. Vassilevski PS, Villa U. A mixed formulation for the Brinkman problem. *SIAM Journal on Numerical Analysis* 2014; **52**(1):258–281.
20. Brezzi F, Fortin M. *Mixed and Hybrid Finite Element Methods*. Springer Verlag: New York, 1991.
21. Franca LP, Hughes TJR. Two classes of mixed finite element methods. *Computer Methods in Applied Mechanics and Engineering* 1988; **69**(1):89–129.
22. Gatica GN. Analysis of a new augmented mixed finite element method for linear elasticity allowing $\mathbb{RT}_0-\mathbb{P}_1-\mathbb{P}_0$ approximations. *ESAIM: Mathematical Modelling and Numerical Analysis* 2006; **40**(1):1–28.
23. Gatica GN. *A Simple Introduction to the Mixed Finite Element Method. Theory and Applications*, Springer Briefs in Mathematics. Springer: Cham Heidelberg New York Dordrecht London, 2014.
24. Anaya V, Mora D, Ruiz-Baier R. An augmented mixed finite element method for the vorticity-velocity-pressure formulation of the Stokes equations. *Computer Methods in Applied Mechanics and Engineering* 2013; **267**:261–274.
25. Figueroa LE, Gatica GN, Heuer N. A priori and a posteriori error analysis of an augmented mixed finite element method for incompressible fluid flows. *Computer Methods in Applied Mechanics and Engineering* 2008; **198**(2): 280–291.
26. Figueroa LE, Gatica GN, Márquez A. Augmented mixed finite element methods for the stationary Stokes equations. *SIAM Journal of Scientific Computing* 2008; **31**(2):1082–1119.
27. Gatica GN, Gatica LF, Márquez A. Augmented mixed finite element methods for a vorticity-based velocity–pressure–stress formulation of the Stokes problem in 2D. *International Journal for Numerical Methods in Fluids* 2011; **67**(4):450–477.
28. Gatica GN, Márquez A, Oyarzúa R, Rebolledo R. Analysis of an augmented fully-mixed approach for the coupling of quasi-Newtonian fluids and porous media. *Computer Methods in Applied Mechanics and Engineering* 2014; **270**(1):76–112.
29. Heys JJ, Lee E, Manteuffel TA, McCormick SF, Ruge JW. Enhanced mass conservation in least-squares methods for Navier-Stokes equations. *SIAM Journal of Scientific Computing* 2009; **31**:2303–2321.

30. Barrios TP, Gatica GN. An augmented mixed finite element method with Lagrange multipliers: a priori and a posteriori error analyses. *Journal of Computational and Applied Mathematics* 2007; **200**(2):653–676.

31. Gatica GN. Solvability and Galerkin approximations of a class of nonlinear operator equations. *Zeitschrift fur Analysis und ihre Anwendungen* 2002; **21**(3):761–781.

32. Gatica GN, Heuer N, Meddahi S. On the numerical analysis of nonlinear two-fold saddle point problems. *IMA Journal on Numerical Analysis* 2003; **23**(2):301–330.

33. Bochev PV. Analysis of least-squares finite element methods for the Navier–Stokes equations. *SIAM Journal on Numerical Analysis* 1997; **34**(5):1817–1844.

34. Jiang B. *The Least-Squares Finite Element Method. Theory and Applications in Computational Fluid Dynamics and Electromagnetics. Scientific Computation.* Springer Verlag: Berlin, 1998. xvi+418 pp.

35. Ciarlet PG. The Finite Element Method for Elliptic Problems. In *Studies in Mathematics and its Applications*, Vol. 4. North-Holland Publishing Co.: Amsterdam-New York-Oxford, 1978. xix+530 pp.

36. Clément P. Approximation by finite element functions using local regularisation. *RAIRO. Modélisation Mathématique et Analyse Numérique* 1975; **9**:77–84.

37. Carstensen C. A-posteriori error estimate for the mixed finite element method. *Mathematics of Computation* 1997; **66**(218):465–476.

38. Verfürth R. *A Review of A posteriori Error Estimation and Adaptive Mesh-Refinement Techniques.* 129 pp. Wiley-Teubner: Chichester - New York - Stuttggart, 1996.

39. Verfürth R. A posteriori error estimation and adaptive mesh-refinement techniques. *Journal of Computational and Applied Mathematics* 1994; **50**(1–3):67–83.

40. Barrios TP, Gatica GN, González GNM, Heuer N. A residual based a posteriori error estimator for an augmented mixed finite element method in linear elasticity. *ESAIM: Mathematical Modelling and Numerical Analysis* 2006; **40**(5):843–869.

41. Gatica GN, Ruiz-Baier R, Tierra G. A mixed finite element method for Darcy's equations with pressure dependent porosity. *Mathematics of Computation,* to appear.

42. Gornak T, Guermond JL, Iliev O, Minev PD. A direction splitting approach for incompressible Brinkman flow. *International Journal of Numerical Analysis and Modeling B* 2013; **4**(1):1–13.